Article

Origin of complexity in haemoglobin evolution

https://doi.org/10.1038/s41586-020-2292-y

Received: 30 July 2019

Accepted: 7 April 2020

Published online: 20 May 2020

Check for updates

Arvind S. Pillai[1], Shane A. Chandler[2,8], Yang Liu[3,8], Anthony V. Signore[4,8], Carlos R. Cortez-Romero[5], Justin L. P. Benesch[2], Arthur Laganowsky[3], Jay F. Storz[4], Georg K. A. Hochberg[1,7] & Joseph W. Thornton[1,6]✉

Most proteins associate into multimeric complexes with specific architectures[1,2], which often have functional properties such as cooperative ligand binding or allosteric regulation[3]. No detailed knowledge is available about how any multimer and its functions arose during evolution. Here we use ancestral protein reconstruction and biophysical assays to elucidate the origins of vertebrate haemoglobin, a heterotetramer of paralogous α- and β-subunits that mediates respiratory oxygen transport and exchange by cooperatively binding oxygen with moderate affinity. We show that modern haemoglobin evolved from an ancient monomer and characterize the historical 'missing link' through which the modern tetramer evolved—a noncooperative homodimer with high oxygen affinity that existed before the gene duplication that generated distinct α- and β-subunits. Reintroducing just two post-duplication historical substitutions into the ancestral protein is sufficient to cause strong tetramerization by creating favourable contacts with more ancient residues on the opposing subunit. These surface substitutions markedly reduce oxygen affinity and even confer cooperativity, because an ancient linkage between the oxygen binding site and the multimerization interface was already an intrinsic feature of the protein's structure. Our findings establish that evolution can produce new complex molecular structures and functions via simple genetic mechanisms that recruit existing biophysical features into higher-level architectures.

The interfaces that hold molecular complexes together typically involve sterically tight, electrostatically complementary interactions among many amino acids[4]. Similarly, allostery and cooperativity usually depend on numerous residues that connect surfaces to active sites[5]. The acquisition of such complicated machinery would seem to require elaborate evolutionary pathways. The classical explanation of this process, by analogy to the evolution of morphological complexity, is that multimerization conferred or enhanced beneficial functions, allowing selection to drive the many substitutions required to build and optimize new interfaces[4,6].

Whether this account accurately describes the evolution of any natural molecular complex requires a detailed reconstruction of the historical steps by which it evolved. Haemoglobin (Hb) is a useful model for this purpose, because the structural mechanisms that mediate its multimeric assembly, cooperative oxygen binding, and allosteric regulation are well established[7,8]. Moreover, its subunits descend by duplication and divergence from the same ancestral proteins, so their history can be reconstructed in a single analysis. Despite considerable speculation[9–11], virtually nothing is known about the evolutionary origin of Hb's heterotetrameric architecture and the functions that depend on it.

From monomer to homodimer

We inferred the phylogeny of Hb and closely related globins (Fig. 1a, Extended Data Fig. 1a, b, e). The duplication that produced the distinct Hbα and Hbβ subunits occurred before the last common ancestor of jawed vertebrates (Fig. 1a). The closest outgroups—myoglobin (Mb)[12], globin E[13], and globin Y (Extended Data Fig. 1d)—are monomers. A more distant clade of agnathan 'haemoglobin' and vertebrate cytoglobin includes monomers and dimers[14,15], but the dimers assemble through interfaces that differ from each other and from those used in Hb, indicating parallel acquisition[16,17]. These observations suggest that the Hb $\alpha_2\beta_2$ heterotetramer evolved from an ancestral monomer via an unknown intermediate form.

To characterize when and how the tetramer evolved, we first reconstructed Hb of the ancestral jawed vertebrate by phylogenetically inferring the maximum a posteriori sequences of the ancestral α- and β-subunits (Ancα and Ancβ; Fig. 1a, Extended Data Fig. 1b, c). We coexpressed and purified Ancα and Ancβ and characterized their assembly using native mass spectrometry (nMS), size-exclusion chromatography (SEC) and multi-angle light scattering (MALS). Like extant Hb, Ancα and Ancβ associate into $\alpha_2\beta_2$ heterotetramers, with a tetramer–dimer

[1]Department of Ecology and Evolution, University of Chicago, Chicago, IL, USA. [2]Department of Chemistry, Chemistry Research Laboratory, University of Oxford, Oxford, UK. [3]Department of Chemistry, Texas A&M University, College Station, TX, USA. [4]School of Biological Sciences, University of Nebraska, Lincoln, NE, USA. [5]Program in Cell and Molecular Biology, University of Chicago, Chicago, IL, USA. [6]Department of Human Genetics, University of Chicago, Chicago, IL, USA. [7]Present address: Max Planck Institute for Terrestrial Microbiology, Marburg, Germany. [8]These authors contributed equally: Shane A. Chandler, Yang Liu, Anthony V. Signore. ✉e-mail: joet1@uchicago.edu

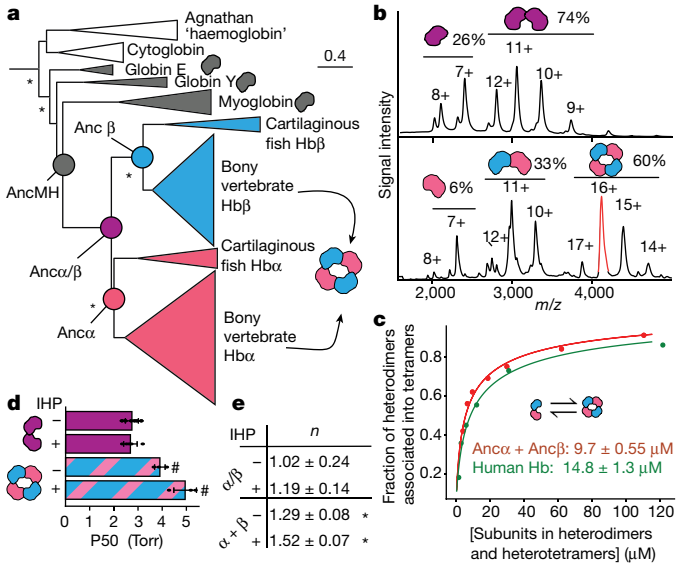

Fig. 1 | Structure and function of ancestral globins. a, Simplified phylogeny of vertebrate globins. Icons, oligomeric states. *Approximate likelihood ratio statistic >10. Complete phylogeny in Extended Data Fig. 1a. Circles, reconstructed ancestral proteins. Scale bar, substitutions per site. **b**, nMS spectra of Ancα/β (top, purple) and Ancα + Ancβ (lower, pink and blue) at 20 μM. Charge states, stoichiometries, and occupancy (fraction of moles of subunits) shown. Red, analysed by tandem mass spectrometry (MS/MS) in Extended Data Fig. 2e. **c**, Dimer-to-tetramer affinity of Ancα + Ancβ (red) and human Hb (green). Circles, fraction of α + β heterodimers incorporated into $\alpha_2\beta_2$ tetramers, measured once by nMS. K_d ± s.e. (in moles of subunits) estimated by nonlinear regression. **d**, **e**, Oxygen affinity (P50) and cooperativity (Hill coefficient, *n*) of Ancα/β and Ancα + Ancβ. IHP, twofold molar excess of inositol hexaphosphate. Mean ± 95% confidence interval (CI) from 3–5 replicates (dots) shown. #, P50 significantly different from Ancα/β under corresponding conditions ($P < 0.01$, *t*-test). *Significant cooperativity ($n \neq 1$, $P < 0.05$, *F*-test; Extended Data Fig. 1f).

dissociation constant (K_d) of 10 μM, comparable to that of human Hb (15 μM; Fig. 1b, c, Extended Data Fig. 2a–c, f, i). Expressed in isolation, Ancα forms homodimers (Extended Data Fig. 3a), and Ancβ forms homotetramers (Extended Data Fig. 3b), just as extant Hb subunits do[18,19]. The heterotetrameric structure of Hb therefore evolved before the jawed vertebrate ancestor, more than 400 million years ago.

By contrast, Ancα/β, the pre-duplication ancestral protein, homodimerizes with a K_d of 9 μM measured by nMS, but does not form tetramers (Fig. 1b, Extended Data Fig. 2d, f, g). Even at 1.4 mM, no tetramers are detectable using SEC (Extended Data Fig. 2h). Ancα/β was therefore a homodimer, with virtually no propensity to tetramerize. This result is robust even when we incorporate statistical uncertainty about the ancestral sequence in several alternative constructs (Extended Data Fig. 4). This is also the most parsimonious history, because extant Hbα dimerizes and Hbβ tetramerizes when they are expressed in isolation[18,19]: a monomeric Ancα/β would imply independent gains of dimerization, and a tetramer would require early gain of tetramerization followed by loss in Hbα (Extended Data Fig. 4).

AncMH, the common ancestor of Hb and myoglobin, is monomeric. No higher-order stoichiometries were detected using nMS of His-tagged AncMH at 70 μM (Extended Data Fig. 3f). Even at 600 μM, only monomers were apparent using SEC (Extended Data Fig. 2j). The untagged protein also does not dimerize at concentrations at which Ancα/β is predominantly dimeric, as shown using SEC and a globin-specific concentration assay on lysate from transformed cells (Extended Data Fig. 3d, e). A monomeric AncMH is also the most parsimonious scenario, because its closest outgroups are all monomers (Extended Data Fig. 4b–e).

The Ancα/β homodimer is therefore the evolutionary missing link between an ancient monomer and the Hb heterotetramer. After duplication, a novel interaction evolved, enabling these dimers to associate into tetramers.

Evolution of Hb functions

We characterized the evolution of the functional properties of Hb by assaying the oxygen-binding characteristics of the ancestral proteins. The physiological role of modern Hb—loading oxygen in the lungs or gills and unloading it in the periphery—is possible because Hb binds and releases oxygen cooperatively and has an affinity lower than that of myoglobin; its affinity is further reduced by allosteric effectors[8]. Like human Hb, the coexpressed and copurified complex Ancα + Ancβ displays measurable cooperativity, and its oxygen affinity is similar to that of stripped, recombinant human Hb[20] (Fig. 1d, e). The affinity of Ancα + Ancβ is reduced in the presence of the allosteric effector inositol hexaphosphate (IHP), although by less than that of human Hb[20]. The functional characteristics of extant Hb were therefore in place by the jawed vertebrate ancestor.

By contrast, the oxygen affinity of Ancα/β is significantly higher than that of Ancα + Ancβ, and it does not display detectable cooperativity or allosteric regulation by IHP (Fig. 1d, e, Supplementary Discussion). The major functional characteristics of modern Hb therefore evolved between Ancα/β and Ancα + Ancβ, the same interval during which tetramerization evolved. This also represents the most parsimonious history: Hb tetramers are cooperative, but Hbα homodimers and Hbβ homotetramers are not[18,21], suggesting that this property did not yet exist in their common ancestor (Extended Data Fig. 4).

Because Ancα/β lacked cooperativity, allostery, or reduced affinity, it could not have performed modern Hb's physiological role in oxygen exchange. Furthermore, the first step in the evolution of Hb's tetrameric architecture—acquisition of homodimerization from a monomeric ancestor—could not have been driven by selection for the major functional properties of Hb, because the homodimer did not possess any of them.

Ancestral and derived interfaces

Hb assembles via two distinct interfaces on each subunit: IF1 mediates α1–β1 and α2–β2 contacts, while IF2 mediates α1–β2 and α2–β1 contacts[7] (Fig. 2a). To determine which interface evolved before Ancα/β, we applied hydrogen–deuterium exchange mass spectrometry (HDX-MS) to Ancα/β. We compared patterns of deuterium uptake at high and low protein concentrations (at which dimers or monomers predominate, respectively; Extended Data Fig. 2d, f, g). Solvent-exposed residues incorporate deuterium faster than buried residues, so peptides that contribute to the dimer interface should exhibit higher deuterium uptake when the monomeric state predominates. We found that Ancα/β peptides containing residues in IF1 incorporate significantly more deuterium under monomer-favouring than dimer-favouring conditions; no difference was observed for IF2 (Fig. 2b, c, Extended Data Figs. 5–8). Moreover, mutations in residues in IF1 substantially impair dimerization of Ancα/β, but a mutation that disrupts IF2 in human Hb[22] has no effect (Fig. 2d, Extended Data Figs. 7c, 9). Reverting all IF1 residues in Ancα/β to the amino acid state from AncMH yields predominantly monomers, but reverting those at IF2 has no effect (Fig. 2d, Extended Data Fig. 7d).

Ancα/β homodimers therefore assembled via IF1. After duplication, IF2 evolved, enabling dimers to assemble into tetramers (Fig. 2e). Corroborating this inference, extant Hbα homodimers assemble via IF1, whereas Hbβ tetramers use both IF1 and IF2, indicating that IF1 was inherited from their ancestor Ancα/β[18,19]. The finding that IF2 evolved after the gene duplication explains why Ancα/β is neither cooperative nor allosterically regulated, because both functions require IF2-mediated assembly into tetramers[23].

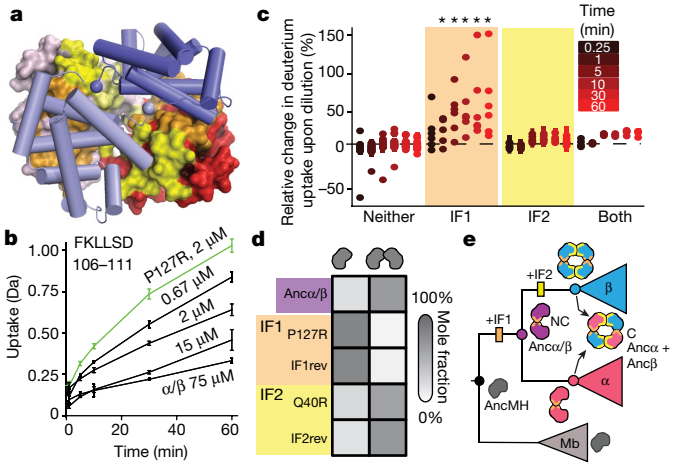

Fig. 2 | Identification of homodimerization interface in Ancα/β. a, Hb heterotetramers assemble via two interfaces (IF1, orange; IF2, yellow) on each subunit. Red and pink surfaces, α-subunits; blue cartoon, β-subunits. Ancα + Ancβ homology model is shown. **b**, Deuterium incorporation by an Ancα/β peptide that contributes to IF1 (Extended Data Fig. 5g, h). Uptake (mean ± s.e. from three replicates per incubation time) is shown for Ancα/β (black) and monomeric IF1 mutant P127R (green). **c**, Each circle shows mean difference in deuterium uptake by one Ancα/β peptide when expressed at monomer-favouring versus dimer-favouring concentrations (0.67 and 75 μM, respectively; three replicates each, with s.e.). Peptides are classified by the interface to which they contribute and coloured by incubation time. *Mean uptake in interface category significantly different from other categories ($P < 0.05$, permutation test, Extended Data Figs. 6g, 7). **d**, Dimer and monomer occupancy by Ancα/β and mutants, assessed using nMS at 20 μM. P127R and Q40R disrupt IF1 and IF2, respectively. IF1rev and IF2rev revert historical substitutions to state in AncMH (spectra in Extended Data Fig. 7c, d). **e**, Evolution of Hb tetramer. Rectangles, acquisition of IF1 and IF2. C, cooperative; NC, noncooperative; Mb, myoglobin.

Genetic mechanisms for the new interface

The causal substitutions for the evolution of heterotetramers from the homodimer must have occurred on one or both of the post-duplication branches that lead from Ancα/β to Ancα and Ancβ. On the Ancα branch, there were only three changes, of which none were at IF2. On the Ancβ branch, there were 42 changes, including 5 at IF2 and 4 others at IF1 (Fig. 3a, b).

We introduced the IF2 substitutions into Ancα/β (Ancα/β5) and found that they confer strong assembly into tetramers when Ancα/β5 is coexpressed with Ancα; the mixture includes both heterotetramers and homotetramers (Fig. 3c, Extended Data Fig. 10c, d). A version containing only four of the substitutions (Ancα/β4) formed homotetramers at 20 μM but did not heteromerize with Ancα. The fifth change (H104E) therefore confers the capacity to associate with Ancα, probably because it interacts with His104 on Ancα, forming a hydrogen bond in the heteromer but clashing in the homomer (Fig. 3c, Extended Data Fig. 10a, b). Even a subset of just two IF2 changes (Ancα/β2) causes high-affinity assembly into homotetramers ($K_d = 1$ μM; Fig. 3c, e, Extended Data Fig. 10g). The genetic basis for the evolution of a new strong interface was therefore simple.

The IF2 substitutions are not sufficient to yield specific occupancy of the $\alpha_2\beta_2$ architecture: coexpressing Ancα/β5 with Ancα produces a mixture of tetramers containing zero, one, or two α-subunits (Fig. 3c, Extended Data Fig. 10c, d). We hypothesized that IF1 substitutions conferred heterospecificity by favouring the assembly of heterodimers across IF1, which then form $\alpha_2\beta_2$ heterotetramers across IF2. We introduced the IF1 substitutions into Ancα/β5 (Ancα/β9) and coexpressed it with Ancα. As predicted, heterotetramers and heterodimers predominate over homomers (Fig. 3d). Ancα/β9 + Ancα is poorly soluble, preventing quantification by nMS, but the addition of five historical

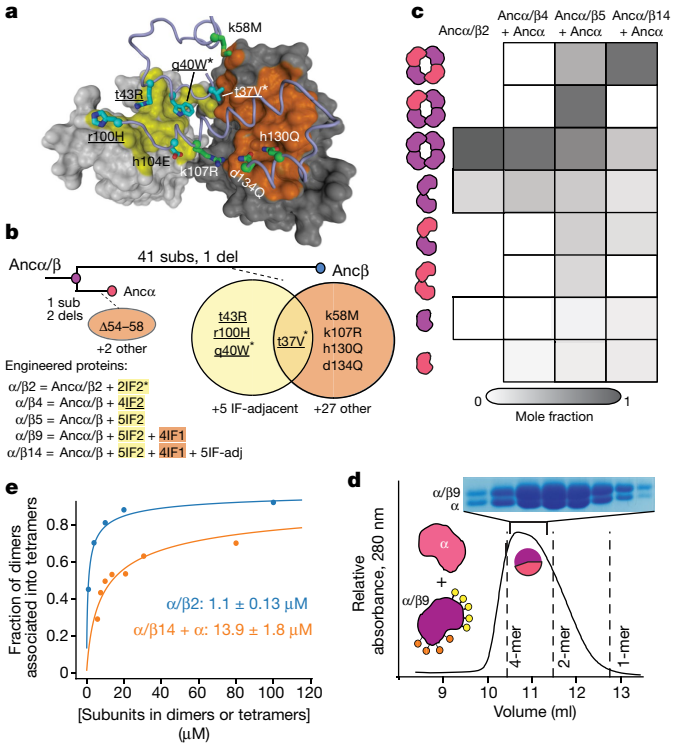

Fig. 3 | Genetic mechanisms of tetramer evolution. a, Homology model of Ancα + Ancβ tetramer with interface residues substituted between Ancα/β and Ancβ. Grey surfaces, two Ancα subunits; yellow, IF2; orange, IF1. Blue cartoon, partial backbone of one Ancβ subunit; sticks, side chains of substituted sites (cyan, IF2; green, IF1). Labels show state in Ancα/β (lowercase) and Ancβ (uppercase). *Sites in Ancα/β2; underlined, sites in Ancα/β4. **b**, Phylogenetic interval between Ancα/β and Ancα + Ancβ with number of substitutions and deletions per branch. Venn diagrams, sites substituted at interfaces. Below, substitutions incorporated in mutant proteins. **c**, Occupancy of multimers measured by nMS at 20 μM, as fraction of moles of subunits in each state. Ancα/β2 was expressed in isolation, so only homomers are plotted. Spectra in Extended Data Fig. 10. **d**, SEC of Ancα/β9 + Ancα at 80 μM. Lines, elution volumes of tetramer (Ancα + Ancβ), dimer (Ancα/β), monomer (human Mb). Pie chart, proportions of Ancα and Ancα/β9 subunits in tetramer-containing fraction, measured by denaturing MS (Extended Data Fig. 11e). Top, electrophoresis of tetramer-containing fraction. **e**, Dimer-to-tetramer affinity of Ancα/β2 (blue) and Ancα/β14 + Ancα (orange). Orange circles, fraction of Ancα/β14 + Ancα heterodimers incorporated into heterotetramers; blue, fraction of Ancα/β2 homodimers in homotetramers, measured by nMS once. K_d ± s.e. estimated by nonlinear regression.

substitutions at sites proximal to the interfaces (Ancα/β14 + Ancα) improves solubility, and nMS confirmed preferential occupancy of $\alpha_2\beta_2$ heterotetramers ($K_d = 14$ μM; Fig. 3c, e, Extended Data Fig. 10e, f).

The Hb heterotetramer therefore evolved from the Ancα/β homodimer via two sets of substitutions. Changes at IF2 created a strong new interface that conferred tetramerization; changes at IF1 yielded heterospecificity. In both cases, only a few substitutions were required.

Structural mechanisms for the new interface

We next investigated how so few substitutions could have generated a new and specific multimeric interaction. Using a homology model of the heterotetramer, we identified all favourable contacts that mediate association across the ancestral interfaces and used the phylogeny to determine when these amino acids evolved (Fig. 4a–c, Extended Data Fig. 10h, i).

The substitutions that conferred tetramerization recruited residues that already existed on the opposing surface into newly favourable interactions. All 13 residues that Ancα contributes to IF2 are unchanged from

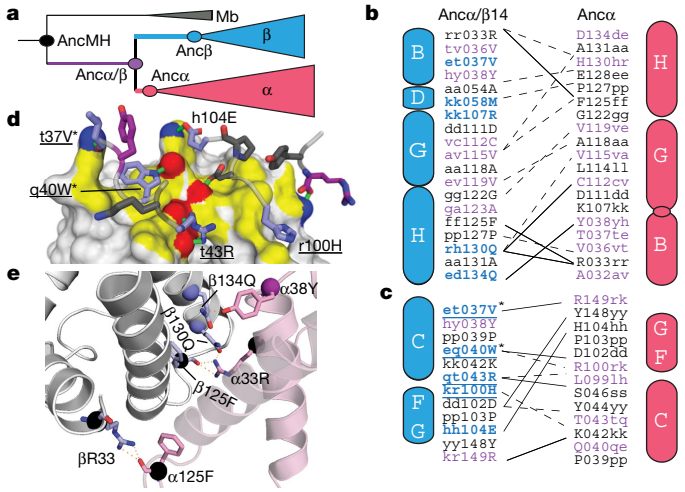

Fig. 4 | Structural mechanisms of evolution of Hb interfaces. a, Phylogenetic classification of ancestral states and substitutions. Black, state in AncMH; purple, substituted from AncMH to Ancα/β; blue or red, substituted from Ancα/β to Ancβ or Ancα. **b**, **c**, Contact maps for residues buried at IF1 (**b**) and IF2 (**c**) of Ancα + Ancβ. Residues coloured by scheme in **a**. Letters show state in AncMH (outside, lower case), Ancα/β (middle, lower case) and Ancβ or Ancα (inside, upper case). Solid lines, predicted hydrogen bonds; dashed lines, van der Waals interactions. Underlined, substitutions in Ancα/β4; *substitutions in Ancα/β2. Cylinders, helices (Extended Data Fig. 2a). Oval, deletion of helix D in Ancα. **d**, IF2 contacts in Ancα + Ancβ. Grey surface, Ancα, with yellow IF2; hydrogen-bonding atoms are red (oxygen) or blue (nitrogen), with bonds as green lines. Cartoon, Ancβ backbone, with IF2-interacting sidechains (sticks, coloured as in **a**). **e**, Close-up of IF1 in Ancα + Ancβ model. Sticks, hydrogen-bonding residues; spheres, Cα atoms; coloured as in **a**.

their ancestral state in Ancα/β, and many were acquired earlier (Fig. 4c). The IF2 substitutions on the Ancβ branch yielded new van der Waals contacts and hydrogen bonds with these ancient residues (Fig. 4c, d). For example, the ring of Trp40 (substituted in Ancβ from the ancestral glutamine) nestles tightly in an ancient hydrophobic indentation on Ancα. Similarly, the IF1 substitutions that increase occupancy of the $\alpha_2\beta_2$ heterotetramer all modify interactions with ancient residues that were conserved on Ancα (Fig. 4b, e).

Both interfaces also involve favourable contacts between residues that were unchanged from their deep ancestral states in both subunits. In IF1, for example, R33 on each subunit donates two hydrogen bonds to F125 on the facing surface, and both residues evolved before AncMH. Each subunit contains both residues, and IF1 occurs twice in the tetramer, so these two sites form a total of eight hydrogen bonds in the complex (Fig. 4b, e). Similarly, IF2 contains several hydrogen bonds and Van der Waals interactions between pairs of residues that originated before Ancα/β.

Because of the exponential relationship between binding energy and affinity, one substitution can markedly increase the occupancy of the multimer, if it builds on the foundation of even very weak interactions between older residues. Satisfying an unpaired hydrogen-bond donor or acceptor or burying a hydrophobic ring can contribute up to 16 kJ mol^{-1} to an association[24,25]. Each interface occurs twice in Hb (Fig. 2a), so a substitution that confers a favourable interaction does so twice in the tetramer, doubling its effect on binding free energy and reducing K_d by up to six orders of magnitude. A single mutation can therefore shift occupancy of the tetramer from virtually nonexistent to the predominant species.

Mechanisms of cooperativity

Finally, we sought insight into the evolution of the cooperativity and reduced affinity of Ancα + Ancβ. Cooperativity in extant Hb involves two conformational states that all subunits can adopt: one has higher affinity for oxygen but weaker IF2 contacts between subunits than the other[23,26]. Cooperativity is classically thought to be mediated by an 'allosteric core'—the set of residues on the helix that connect the haem to IF2, which is positioned differently in the two conformations[27].

To understand the mechanisms that triggered the evolution of cooperativity and reduced oxygen affinity, we first examined the phylogenetic history of residues in the haem pocket and allosteric core. At sites within 4 Å of the haem, no substitutions occurred during the interval when cooperativity was acquired. The vast majority were acquired before AncMH (Fig. 5a, Extended Data Fig. 1c), including the proximal histidine, which covalently binds the haem iron and transduces the movement of the haem upon oxygen binding to the allosteric core and IF2, thereby causing the other subunits to shift between low- and high-affinity conformations. Two substitutions occurred in Ancβ on the helix that connects IF2 to the histidine, but there were none in Ancα (Fig. 5a), and both subunits make the conformational transition in extant Hb. These observations suggest that the structural properties that mediate the allosteric linkage between the haem–oxygen-binding site and IF2 already existed in Ancα/β, before cooperativity and tetramerization evolved. Consistent with this idea, many of the conformational changes that mediate Hb cooperativity, such as distortion of the haem's geometry and movement of the histidine and helix upon oxygen binding, also occur in myoglobin, which is monomeric and noncooperative[28,29].

We hypothesized that, because of this ancient structural connection between the IF2 surface and the active site, evolution of the intersubunit interaction across IF2 was sufficient to confer cooperativity and reduce affinity. We characterized oxygen binding by Ancα/β2, which contains only two historical substitutions at IF2. As predicted, we found that these mutations reduce oxygen affinity by two- to threefold compared to Ancα/β (Fig. 5b); they also confer weak but statistically significant cooperativity (Extended Data Fig. 5b). Acquisition of the tetrameric association alone therefore changes the oxygen-binding function of the protein and confers cooperative oxygen binding.

The tetramer's ability to transition between high- and low-affinity states, however, is sensitive to mutation. Ancα/β4 and the Ancα/β14 + Ancα heterotetramer also have reduced oxygen affinity relative to Ancα/β, but they lose the cooperativity found in Ancα/β2 (Fig. 5b). A likely explanation is that the additional mutations in these constructs overstabilize the low-affinity conformation relative to the high-affinity state. If so, then some of the other substitutions that occurred between Ancα/β and the cooperative complex Ancα + Ancβ must have tuned this equilibrium so that both conformations can be occupied, depending on the oxygen partial pressure (Fig. 5c). The order in which these changes occurred cannot be resolved: the IF2 substitutions may have immediately generated a cooperative Hb-like complex, similar to Ancα/β2; alternatively, cooperativity may have evolved via a low-affinity tetrameric intermediate, like Ancα/β4 (Fig. 5c).

Evolution of molecular complexity

Our findings establish that a few genetic changes drove the evolution of Hb's complex structure and functions from its dimeric precursor. Other molecular complexes may also have evolved by short mutational paths. Interactions between proteins and other kinds of substrates, such as DNA or small molecules, have historically evolved via one or a few historical substitutions[30], and we see no reason why multimeric interactions in general should be more difficult to evolve. Multimers can be engineered from non-assembling precursors by one or a few mutations[31,32], and naturally occurring point mutations are known to cause disease by inducing higher-order complexes[33].

The simple mechanism by which Hb appears to have evolved its cooperativity—acquisition of binding to a molecular partner at a new interface—could explain the origin of cooperativity and allostery in

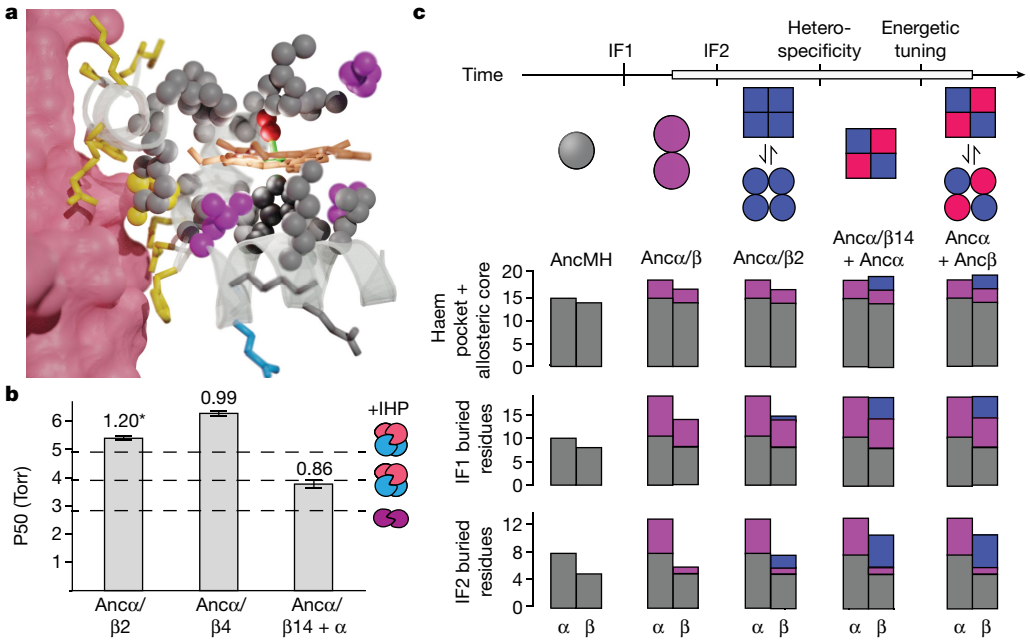

Fig. 5 | Evolution of cooperativity by interface acquisition. a, Haem pocket and IF2 in Ancα + Ancβ. Pink surface, one Ancα. Tan sticks, haem (with green iron and red oxygen). Spheres, Ancβ residues within 4 Å of haem, coloured by temporal category: grey, conserved since AncMH (dark grey, iron-coordinating histidine); purple, conserved since Ancα/β; blue, substituted between Ancα/β and Ancβ. Sticks, other residues on helix connecting histidine to IF2, coloured temporally. Yellow, Ancβ residues at IF2. No changes near haem or IF2 occurred in Ancα. **b**, Oxygen binding by Ancα/β mutants with historical substitutions. P50 ± SE, with Hill coefficient *n* above, estimated by nonlinear regression under effector-stripped conditions (raw data in Extended Data Fig. 10j). *Significant cooperativity ($n \neq 1$, $P \leq 0.05$, *F*-test, Extended Data Fig. 1f). Dotted lines, affinities of Ancα + Ancβ and Ancα/β, which is unaffected by IHP. **c**, Top, evolution of the cooperative Hb heterotetramer. Circles and squares, conformations with high and low oxygen affinity, respectively. Two IF2 substitutions cause homotetramerization, cooperativity, and reduced affinity (**b**). Other substitutions that confer heterotetramerization change the relative stabilities of high and low-affinity conformations, abolishing or restoring cooperativity. White box, interval in which order of substitutions is unknown. Bottom, acquisition of residues in structurally defined categories in Ancα and Ancβ, coloured by temporal category. No changed occurred in Ancα.

other systems[34,35]. If two plausible conditions are met—the new interface is near or structurally connected to the functionally active site, and the optimal conformation for binding is different from the optimal conformation for activity—then binding will impair activity, and vice versa. Given this tradeoff, the evolution of binding alone will confer cooperativity or negative allostery.

The history of Hb shows that complex molecular structures and functions can arise by means other than the long, gradual trajectories of functional optimization by which biological complexity has long been thought to evolve[6,36]. In principle, molecular assemblies could arise and become more complex via neutral processes[37–39], but this scenario is unlikely if many mutations are required. Our work shows that the higher-level multimeric state and functional properties of Hb evolved through just a few mutations, which fortuitously built upon and interacted with ancient structural features. These older features could not have been initially acquired because of selection for the functions of the final complex, because they existed before those functions first appeared. Some are likely to have originated and been preserved by selection for more ancient functions, while others may have appeared transiently by chance. Although evolution of any particular molecular sequence or architecture without consistent selection for those properties is vanishingly improbable, our findings suggest that proteins evolve constantly through a dense space of possibilities in which complex new interactions and functional states are easily accessible.

Online content

Any methods, additional references, Nature Research reporting summaries, source data, extended data, supplementary information, acknowledgements, peer review information; details of author contributions and competing interests; and statements of data and code availability are available at https://doi.org/10.1038/s41586-020-2292-y.

1. Ahnert, S. E., Marsh, J. A., Hernández, H., Robinson, C. V. & Teichmann, S. A. Principles of assembly reveal a periodic table of protein complexes. *Science* **350**, aaa2245 (2015).
2. Marsh, J. A. & Teichmann, S. A. Structure, dynamics, assembly, and evolution of protein complexes. *Annu. Rev. Biochem.* **84**, 551–575 (2015).
3. Monod, J., Wyman, J. & Changeux, J. P. On the nature of allosteric transitions: a plausible model. *J. Mol. Biol.* **12**, 88–118 (1965).
4. Goodsell, D. S. & Olson, A. J. Structural symmetry and protein function. *Annu. Rev. Biophys. Biomol. Struct.* **29**, 105–153 (2000).
5. Rivalta, I. et al. Allosteric pathways in imidazole glycerol phosphate synthase. *Proc. Natl Acad. Sci. USA* **109**, E1428–E1436 (2012).
6. Dawkins, R. *Climbing Mount Improbable* (WW Norton & Company, 1997).
7. Perutz, M. F. et al. Structure of haemoglobin: a three-dimensional Fourier synthesis at 5.5-A. resolution, obtained by X-ray analysis. *Nature* **185**, 416–422 (1960).
8. Storz, J. F. *Hemoglobin: Insights into Protein Structure, Function, and Evolution* (Oxford Univ. Press, 2018).
9. Goodman, M. & Moore, G. W. Phylogeny of hemoglobin. *Syst. Zool.* **22**, 508–532 (1973).
10. Coates, M. L. Hemoglobin function in the vertebrates: an evolutionary model. *J. Mol. Evol.* **6**, 285–307 (1975).
11. Zuckerkandl, E. The evolution of hemoglobin. *Sci. Am.* **212**, 110–118 (1965).
12. Kendrew, J. C. et al. Structure of myoglobin: a three-dimensional Fourier synthesis at 2 A. resolution. *Nature* **185**, 422–427 (1960).
13. Blank, M. et al. Oxygen supply from the bird's eye perspective: globin E is a respiratory protein in the chicken retina. *J. Biol. Chem.* **286**, 26507–26515 (2011).
14. Fago, A., Rohlfing, K., Petersen, E. E., Jendroszek, A. & Burmester, T. Functional diversification of sea lamprey globins in evolution and development. *Biochim. Biophys. Acta. Proteins Proteomics* **1866**, 283–291 (2018).
15. Lechauve, C. et al. Cytoglobin conformations and disulfide bond formation. *FEBS J.* **277**, 2696–2704 (2010).
16. Heaslet, H. A. & Royer, W. E., Jr. The 2.7 A crystal structure of deoxygenated hemoglobin from the sea lamprey (*Petromyzon marinus*): structural basis for a lowered oxygen affinity and Bohr effect. *Structure* **7**, 517–526 (1999).
17. Makino, M. et al. High-resolution structure of human cytoglobin: identification of extra N- and C-termini and a new dimerization mode. *Acta Crystallogr. D* **62**, 671–677 (2006).

18. Kidd, R. D., Baker, H. M., Mathews, A. J., Brittain, T. & Baker, E. N. Oligomerization and ligand binding in a homotetrameric hemoglobin: two high-resolution crystal structures of hemoglobin Bart's (γ(4)), a marker for α-thalassemia. *Protein Sci.* **10**, 1739–1749 (2001).
19. Kumar, K. K., Jacques, D. A., Guss, J. M. & Gell, D. A. The structure of α-haemoglobin in complex with a haemoglobin-binding domain from *Staphylococcus aureus* reveals the elusive α-haemoglobin dimerization interface. *Acta Crystallogr. F* **70**, 1032–1037 (2014).
20. Hoffman, S. J. et al. Expression of fully functional tetrameric human hemoglobin in *Escherichia coli*. *Proc. Natl Acad. Sci. USA* **87**, 8521–8525 (1990).
21. Tyuma, I., Benesch, R. E. & Benesch, R. The preparation and properties of the isolated α and β subunits of hemoglobin A. *Biochemistry* **5**, 2957–2962 (1966).
22. Manning, L. R., Dumoulin, A., Jenkins, W. T., Winslow, R. M. & Manning, J. M. Determining subunit dissociation constants in natural and recombinant proteins. *Methods Enzymol.* **306**, 113–129 (1999).
23. Ackers, G. K. Energetics of subunit assembly and ligand binding in human hemoglobin. *Biophys. J.* **32**, 331–346 (1980).
24. Fersht, A. R. et al. Hydrogen bonding and biological specificity analysed by protein engineering. *Nature* **314**, 235–238 (1985).
25. Eisenberg, D. & McLachlan, A. D. Solvation energy in protein folding and binding. *Nature* **319**, 199–203 (1986).
26. Mihailescu, M.-R. & Russu, I. M. A signature of the T → R transition in human hemoglobin. *Proc. Natl Acad. Sci. USA* **98**, 3773–3777 (2001).
27. Gelin, B. R., Lee, A. W. M. & Karplus, M. Hemoglobin tertiary structural change on ligand binding. Its role in the co-operative mechanism. *J. Mol. Biol.* **171**, 489–559 (1983).
28. Sato, A., Gao, Y., Kitagawa, T. & Mizutani, Y. Primary protein response after ligand photodissociation in carbonmonoxy myoglobin. *Proc. Natl Acad. Sci. USA* **104**, 9627–9632 (2007).
29. Barends, T. R. M. et al. Direct observation of ultrafast collective motions in CO myoglobin upon ligand dissociation. *Science* **350**, 445–450 (2015).
30. Siddiq, M. A., Hochberg, G. K. & Thornton, J. W. Evolution of protein specificity: insights from ancestral protein reconstruction. *Curr. Opin. Struct. Biol.* **47**, 113–122 (2017).
31. Garcia-Seisdedos, H., Empereur-Mot, C., Elad, N. & Levy, E. D. Proteins evolve on the edge of supramolecular self-assembly. *Nature* **548**, 244–247 (2017).
32. Grueninger, D. et al. Designed protein-protein association. *Science* **319**, 206–210 (2008).
33. Pauling, L. et al. Sickle cell anemia, a molecular disease. *Science* **110**, 543–548 (1949).
34. Coyle, S. M., Flores, J. & Lim, W. A. Exploitation of latent allostery enables the evolution of new modes of MAP kinase regulation. *Cell* **154**, 875–887 (2013).
35. Reynolds, K. A., McLaughlin, R. N. & Ranganathan, R. Hot spots for allosteric regulation on protein surfaces. *Cell* **147**, 1564–1575 (2011).
36. Darwin, C. *On the Origin of Species by Means of Natural Selection, or the Preservation of Favoured Races in the Struggle for Life* 204–208 (John Murray, 1859).
37. Lynch, M. Evolutionary diversification of the multimeric states of proteins. *Proc. Natl Acad. Sci. USA* **110**, E2821–E2828 (2013).
38. Finnigan, G. C., Hanson-Smith, V., Stevens, T. H. & Thornton, J. W. Evolution of increased complexity in a molecular machine. *Nature* **481**, 360–364 (2012).
39. Gray, M. W., Lukeš, J., Archibald, J. M., Keeling, P. J. & Doolittle, W. F. Irremediable complexity? *Science* **330**, 920–921 (2010).

Methods

Sequence data and alignment

We collected 177 annotated amino acid sequences of haemoglobin and related paralogues in 72 species from UniPROT, Ensembl and NCBI RefSeq. Sequences were aligned using MAFFT v7[40]. The maximum likelihood (ML) phylogeny and branch lengths were inferred from the alignment using PHYML v3.1[41] and the LG model[42] with gamma-distributed among-site rate variation and empirical state frequencies. This best-fit evolutionary model was selected using the Akaike Information Criterion in PROTTEST. Node support was evaluated using the approximate likelihood ratio test statistic (aLRS), which expresses the difference in likelihood between the most likely topology and the most likely topology that does not include the split of interest; aLRS has been shown to be reasonably accurate, robust, and efficient compared to other means of characterizing support[43,44]. The tree was rooted on neuroglobin and globin X, paralogues that are found in both deuterostomes and protostomes[45]. Tetrapods possess three Hbα paralogues, Hbα^{A}, Hbα^{D}, and Hbα^{Z} (also known as Hbα^{E} or Hb-zeta)[46]. The ML phylogeny inferred from this alignment contained a weakly supported sister relationship between all Actinopterygian Hbα genes and the tetrapod Hbα^{Z}, to the exclusion of tetrapod Hbα^{A} and Hbα^{D}. This is a nonparsimonious scenario, because it requires an early gene duplication and subsequent loss of the Hbα^{A}/Hbα^{D} lineage in Actinopterygii. We therefore constrained the topology to unite tetrapod HbαA^{A}, Hbα^{D}, and Hbα^{Z} in a clade (Extended Data Fig. 1a). PhyML v3.1 was then used to re-infer the best-fit branch topology and branch lengths given this constraint.

Ancestral sequences were reconstructed and the posterior probability distributions of ancestral states were inferred using the ML method using the codeml package in PAML 4.9[47], given the ML-constrained phylogeny and branch lengths. Historical substitutions were assigned to phylogenetic branches as differences between the maximum a posteriori amino acid states between parent and daughter nodes. The asymmetry between the branch lengths leading from Ancα/β to Ancα and to Ancβ has been observed previously[48] and presumably reflects there being more shared amino acid states between Hbα and the outgroups (myoglobin, globins E and Y, and so on) than between Hbβ and the outgroups. The sequences for reconstructed ancestors have been deposited in GenBank (IDs MT079112, MT079113, MT079114, MT079115).

Recombinant protein expression

Ancestral genes were codon-optimized for expression in *Escherichi coli* using CodonOpt and generated by de novo DNA synthesis (IDT gBlocks). For globin expression, coding sequences were cloned into a pLIC expression vector without affinity tags and expressed under a T7 polymerase promoter. For oxygen-affinity measurements, plasmid pCOMAP[49], which expresses *E. coli* methionine aminopeptidase 1 (MAP1), was cotransformed to ensure efficient N-terminal methionine excision. For co-expression of two globins, sequences were expressed from a polycistronic operon in plasmid pGM, without tags and under a T7 promoter, separated by a spacer containing a stop codon and ribosome binding site. *E. coli* methionine aminopeptidase 1 (MAP1) was coexpressed from the same plasmid.

JM109 DE3 *E. coli* cells (NEB) were transformed and plated into solid Luria broth (LB) medium containing 50 μg/ml carbenicillin (and 50 μg/ml kanamycin, if pCOMAP was being cotransformed). A single colony was inoculated into 50 ml LB with appropriate antibiotics and grown overnight. Five millilitres of this culture was inoculated into a larger 500-ml LB culture. Cells were grown at 37 °C and shaken at 225 rpm in an incubator (New Brunswick 126) until they reached an optical density at 600 nm (OD600) of 0.4–0.6. The culture was then supplemented with 0.5 mM isopropyl-β-D-1-thiogalactopyranoside (IPTG) and 50 mg/l hemin (Sigma). After 4 h of expression at 37 °C, CO was bubbled through the solution for 10 min and cells were collected by centrifugation at 5,000*g*. Protein purification was carried out immediately after expression.

Protein purification by ion exchange

Ancα/β, P127R, V119A, Ancα/β4 + Ancα and the alternative ancestral reconstructions were purified using ion exchange chromatography[20,49]. All buffers were saturated with CO before purification and vacuum filtered through a 0.2 μM PFTE membrane (Omnipore) to remove particulates. After expression, cells were resuspended in 200 ml of 50 mM Tris (pH 6.8) with 2 cOMPLETE protease inhibitor tablets (Roche) and 0.5 mM DTT. The cell suspension was lysed in 50-ml batches in a glass beaker using an FB505 sonicator with a power setting of 90%, 1 s on/off for 2 min. The lysate was then centrifuged at 30,000*g* to eliminate cell debris, inclusion bodies and aggregates. The supernatant was further syringe-filtered used HPX Millex Durapore filters (Millipore). A HiTrap SP cation exchange (GE) column was attached to an FPLC system (AKTAprime plus) and equilibrated in 50 mM Tris (pH 6.8). Lysate was passed over the column. The SP column was washed with 200 ml of 50 mM Tris to eliminate weakly bound contaminants. Bound Hbs eluted with a 100-ml gradient of 50 mM Tris (pH 6.9) 1 M NaCl, from 0 mM to 1 M. Fractions (0.5 ml) were collected along the length of the gradient. The four reddest fractions were collected and then concentrated in an Amicon μLtra-15 tube by centrifugation at 4,000*g* to a final volume of 500 μl. The sample was injected into a Sephacryl Hiprep 16/60 S-100 HR size-exclusion column (SEC) for additional purification. The column was equilibrated in phosphate buffered saline (PBS) at pH 7.4. Depending on molecular weight, purified globins elute at 48–52 ml (tetramer), 56–60 ml (dimer) or 64–67 ml (monomer). The purity and identity of isolated proteins was assessed using 20% SDS–PAGE and denaturing HRA-MS. The purified proteins were concentrated and then flash frozen with liquid nitrogen until use.

Protein purification by zinc affinity chromatography

Ancα/β5 + Ancα, Ancα/β9 + Ancα, Ancα/β14 + Ancα, and Ancα + Ancβ were purified using zinc-affinity chromatography, adapted from a published method[50]. Buffers were loaded onto the metal affinity column using an AKTAprime FPLC. To prepare the zinc affinity column, nickel was removed from a HisTrap column (GE) using stripping buffer (100 mM EDTA, 100 mM NaCl, 20 mM TRIS, pH 8.0). The column was then washed with diH_2O for five column volumes. Then 0.1 M $ZnSo_4$ was passed over the column until conductance reached a stable value. The column was then washed with five column volumes of water. After expression, cells were resuspended in 50 ml lysis buffer containing 20 mM Tris and 150 mM Nacl (pH 7.4). The cells were sonicated as described above. The lysate was passed over a zinc-affinity HisTrap column. The column was washed with 200 ml wash buffer (20 mM Tris and 150 mM Nacl, pH 7.4). The bound Hbs were eluted with a 50-ml gradient of imidazole, up to 500 mM, and 0.5-ml fractions were collected during the run. The four reddest fractions were collected. The Hb-containing fractions were concentrated and injected into a Sephacryl S-100 HR column for additional purification, as described above.

Purification of globin Y

The globin Y sequences of *Callorhincus milli* (NCBI reference sequence NP_001279719.1) and *Xenopus laevis* (NCBI reference sequence NP_001089155.1) were synthesized (IDT, Coralville, IA, USA) and cloned into a pLIC vector with an N-terminal hexahistidine tag (MHHHHHH). Expression and lysis were carried out under the same conditions as described above. The bacterial lysate was passed over a 5-ml HisTrap nickel-affinity column (GE). The column was washed with five column volumes of wash buffer (20 mM Tris and 150 mM Nacl, pH 7.4). The bound globins were eluted with a 15-ml gradient of imidazole from 0 to 500 mM; five fractions of equal volume were collected. The three reddest fractions were combined. The eluted protein was concentrated to 2 ml, passed through a 0.45-μm filter, and subjected to a final purification

by SEC using a Sephacryl S-100 HR column and an AKTA Prime FPLC system. Globin Y eluted in fractions collected between 61 and 64 ml.

Purification of his-tagged AncMH

The sequence of AncMH was codon-optimized for expression in *E. coli*, synthesized, and cloned into a pLIC vector with an N-terminal hexahistidine tag, because untagged AncMH was not readily purifiable. Recombinant expression, cell lysis, and purification were carried out under the conditions described for globin Y.

Characterization of protein stability

Protein stability was measured by circular dichroism (CD) using a JASCO 1500 CD spectrophotometer. Experiments were conducted at protein concentration of 10 μM (50 mM sodium fluoride, 20 mM sodium phosphate buffer) in a 0.2-mm path length quartz cell. CD spectra were collected at 2 °C intervals (10 min each) as the temperature was increased from 25 °C to 95 °C. Molar ellipticity at 222 nm was measured four times at each temperature; the mean was then divided by the value of molar ellipticity at 222 nm at room temperature (25 °C) to estimate the fraction of unfolded protein. To estimate the melting point (T_m) of each protein, a custom script was written to find the best fit parameters (T_m and slope) for the Boltzmann sigmoid function: fraction unfolded = $1/(1+e^{(t-Tm)/slope)})$. All three ancestral proteins were stable, with $T_m > 60$ °C (Extended Data Fig. 1c).

High-resolution denaturing mass spectrometry

Two hundred microlitres of purified protein was placed in a Slide-A-Lyzer MINI dialysis unit that was suspended in 500 ml of 50 mM ammonium acetate. The solution was stirred overnight at 4 °C. After dialysis, the proteins were transferred to a microfuge tube and centrifuged at 30,000*g* to eliminate aggregates. The concentration was adjusted to 20 μM. Half a microlitre of sample was sprayed using an Agilent 6224 Tof Mass Spectrometer at fragment voltage 200 V. Protein masses were estimated by maximum entropy mass deconvolution implemented in MassHunter (Agilent).

Size-exclusion chromatography and multi-angle light scattering

All proteins were converted to the CO-bound form by adding sodium dithionite to 5 mg/ml, desalting on a Sephadex G-25 desalting column equilibrated with CO-saturated PBS (150 mM NaCl, pH 7.4), and then passing CO through the eluent. Protein concentration was measured by UV absorbance at 280 nm (Tryptophan) and 419 nm (HbCO-specific) using a Nanodrop 2000c (Thermo-scientific). For analytic SEC, a Superdex 75 10/300 GL column (GE) was equilibrated in CO-saturated PBS, and then injected with 500 μl sample, using a 500-μl injection loop on an AKTAprime and monitored by absorbance at 280 nm. For SEC coupled with MALS, a Superdex 200 10/300 GL column was injected with 150 μl sample on the AKTAprime; light scattering and refractive index of eluent were measured using a Dawn Helios-II (Wyatt) light scattering detector and Optilab T-rEX refractometer, respectively. Molar mass fitting was carried out using Astra software.

Globin concentration assay

After protein expression, cells harvested by centrifugation from one 500-ml culture were resuspended in 15 ml PBS and sonicated as described above. Cell debris and aggregate were removed by centrifugation at 20,000*g*. Remaining lysate was concentrated to 5 ml in Amicon μLtra-15 centrifuge concentrators (3,000 NMWL). Five hundred microlitres of this sample was injected into a superdex-75 10/300 GL column. Fractions of eluent (0.2 ml) were collected. We took 50 μl from each fraction and added it to 150 μl Hemoglobin Assay kit reagent (Sigma) in one well of a 96-well plate. In each plate, 50 μl of a 100 mg/dl calibrator (Sigma) was also added to 150 μl of Hemoglobin Assay kit reagent (Sigma) in one well. We used 50 μl PBS added to the 150 μL reagent as a blank. Absorbance was measured at 400 nm using a Victor x5 plate reader (PerkinElmer). Haem concentration in each fraction was measured using the following equation: concentration = $62.5 \times (OD_{sample} - OD_{blank})/(OD_{calibrator} - OD_{blank})$ μM.

Oxygen affinity and cooperativity

Purified proteins were deoxygenated using sodium dithionite at 10 mg/ml and immediately passed through a PD-10 desalting column (GE Healthcare) equilibrated with 25 ml of 0.01 M HEPES/0.5 mM EDTA (pH 7.4). Eluted proteins were concentrated using Amicon μLtra-4 Centrifugal Filter Units (Millipore). Equilibrium oxygen-binding assays were performed at 25 °C using a Blood Oxygen Binding System (Loligo Systems), using 0.1 mM protein (haem concentration) dialysed in 0.1 M HEPES/0.5 mM EDTA buffer. Protein solution was sequentially equilibrated at 3–5 different oxygen tensions (PO_2) yielding 30–70% saturation while continually monitoring absorbance at 430 nm (deoxy peak) and 421 nm (oxy/deoxy isosbestic point). Plots of fractional saturation against PO_2 were constructed from these measurements, and the Hill equation was fit to each plot using OriginPro 2016, yielding estimates of P50 (PO_2 at half-saturation) and the cooperativity coefficient (n, the slope at half saturation in the Hill plot, n50). We collected 95% Cis on parameter estimates by multiplying the s.e.m. over replicate experiments by 1.96 (Fig. 1d, e). The statistical significance of cooperativity was assessed by using an F-test to compare the fit of the data to a model in which n is a free parameter to a null model in which $n = 1$.

To assess the potential for ancestral proteins to have been regulated by allosteric effectors, assays were performed in stripped medium or with IHP added at 0.5 mM. Although IHP may not have been the physiological effector in ancestral organisms, it has been shown to allosterically regulate Hbs from representatives of all major vertebrate lineages, whereas other organic phosphates such as 2,3-biphosphoglycerate (BPG), ATP, and GTP have more lineage-specific effects[51–53]. IHP therefore serves as a useful 'all-purpose' polyanion to test the allosteric regulatory capacity of the ancestral Hb. There is ample precedent for using IHP to study Hb allostery irrespective of whether it is the authentic physiological effector[50,54–56]. This is because IHP modulates $Hb–O_2$ affinity in a manner that is qualitatively similar to those of other effectors, including BPG, ATP, GTP, and IPP[8,50]. These molecules all share the same mechanism of action, reversibly binding a set of cationic residues in the cleft between β_1 and β_2 subunits, and thereby stabilizing the low-affinity T conformation via electrostatic interactions[57–59].

Native mass spectrometry

Proteins were buffer exchanged into 200 mM ammonium acetate with a centrifugal desalting column (Micro Bio-Spin P-6, BioRad) and loaded into a gold-coated glass capillary. Samples were ionized for MS measurement by electrospray ionization. MS and MS/MS ion isolation were performed on a Synapt G1 HDMS instrument (Waters Corporation) equipped with a radio frequency generator to isolate higher m/z species (up to 32k) in the quadrupole, and a temperature-controlled source chamber as previously described[60]. Instrument parameters were tuned to maximize signal intensity for MS and MS/MS while preserving the solution state of the protein complexes. All samples were sprayed at room temperature. Instrument settings were: source temperature of 50 °C, capillary voltage of 1.7 kV, sampling cone voltage of 100 V, extractor cone voltage of 5 V, trap collision energy of 25 V, argon flow rate in the trap set to 7 ml/min (5.6×10^{-2} mbar), and transfer collision energy set to 15 V. The T-wave settings were for trap (300 ms^{-1}/1.0 V), IMS (300 ms^{-1}/20 V) and transfer (100 ms^{-1}/10 V), and trap DC bias (30 V). For MS/MS, ion isolation was achieved using the same settings as described above, with the quadrupole LM resolution set to 6. Activation of protein complexes for individual monomer identification was achieved by increasing the trap collision voltage to 120 V in MS/MS mode, with all other settings unchanged. Analysis of the MS and MS/MS data to estimate masses and relative abundances was performed with the software program Unidec[61].

The occupancy of each stoichiometric state was calculated as the proportion of globin subunits in that state, based on the summed areas under the corresponding peaks in the spectrum. To estimate K_d of the monomer-to-dimer transition Ancα/β, we performed nMS at variable protein concentrations. At each concentration, the observed fraction of subunits incorporated into dimers (F_d) was estimated as $F_d = 2x_d/(x_m + 2x_d)$, where x_m and x_d are the sums of the signal intensities of all peaks corresponding to the monomeric and dimeric stoichiometries, respectively. This procedure was repeated at a range of protein concentrations. Nonlinear regression was then used to find the best-fit value of K_d using the equation

$$F_d = \frac{1}{P_{tot}} \times \frac{(4P_{tot} + K_d) - \sqrt{((4P_{tot} + K_d)^2 - 16P_{tot}{}^2)}}{4}$$

where P_{tot} is the total protein concentration (expressed in terms of monomer) estimated by UV absorbance at 280 nm. The resulting K_d is expressed in terms of the concentration of globin subunits. We observed no higher stoichiometries.

To estimate K_d of the heterodimer–heterotetramer transition in Ancα + Ancβ (or mutant ancestral globins) we performed nMS at variable protein concentrations. Because nMS directly quantifies the abundance of all species in solution, we were able to extract molarities for the α_1/β_1 heterodimer and α_2/β_2 heterotetramers and directly calculate the K_d of their association/dissociation equilibrium, without having to fit a large number of K_d values as part of a coupled set of many equilibria across many homomeric and heteromeric forms. At each concentration, we first calculated the total fraction of subunits that were incorporated into haem-bound heterodimers, including both free heterodimers and heterodimers assembled into heterotetramers, as

$$F_{\alpha\beta} = \frac{2x_{\alpha1\beta1} + 4x_{\alpha2\beta2}}{x_{\alpha1} + x_{\beta1} + 2x_{\alpha1\beta1} + 2x_{\alpha2} + x2_{\beta2} + 4x_{\alpha2\beta2} + 2y_{apo-\alpha1\beta1}}$$

where x is the sum of the signal intensities of all peaks corresponding to the stoichiometry indicated by the subscript. $y_{apo-\alpha1\beta1}$ is the signal intensity of the peaks corresponding to heterodimers that are only partially haem-bound and cannot associate into tetramers. The concentration of all haem-bound subunits incorporated into heterodimers (free heterodimers or assembled into heterotetramers) was calculated as $C_{\alpha\beta} = F_{\alpha\beta} \times P_{tot}$. The fraction of all heterodimers incorporated into heterotetramers was calculated as $F_{\alpha2\beta2} = 4x_{\alpha2\beta2}/(2x_{\alpha1\beta1} + 4x_{\alpha2\beta2})$.

Assembly of heterodimers into heterotetramers as concentration increases was then analysed to find the best-fit value of K_d using nonlinear regression and the following equation:

$$F_{\alpha2\beta2} = \frac{1}{C_{\alpha\beta}} \times \frac{4C_{\alpha\beta} + K_d - \sqrt{\left(4C_{\alpha\beta} + K_d\right)^2 - 16C_{\alpha\beta}{}^2}}{4}$$

The resulting K_d is expressed in terms of the concentration of globin subunits contained in heterodimers and heterotetramers.

For homotetramerization of globins expressed in isolation, the K_d of the dimer–tetramer transition was calculated using a similar approach. The fraction of all subunits incorporated into homodimers (including both free homodimers and those associated into homotetramers) was calculated as $F_d = (2x_d + 4x_t)/(x_m + 2x_d + 4x_t)$, and the concentration of all dimers was calculated as $C_d = F_d \times P_{tot}$. The fraction of all dimers that were incorporated into tetramers was calculated as $F_t = 4x_t/(2x_d + 4x_t)$. Nonlinear regression was then used to fit K_d to the data using the equation

$$F_t = \frac{1}{C_d} \times \frac{4C_d + K_d - \sqrt{(4C_d + K_d)^2 - 16C_d{}^2}}{4}$$

The resulting K_d is expressed in terms of the concentration of globin subunits contained in homodimers and homotetramers. For Fig. 3c, Ancα/β4 was coexpressed with Ancα and fractionated by SEC, and the tetrameric fraction was analysed by nMS.

Native MS spectra for human Hb and Ancα/β14 + Ancα at high concentrations contained peaks corresponding to dimers that had lost one or both haems. In these cases, we calculated K_d values by both including and excluding these species. For the fits shown in Figs. 1d and 3d, these peaks were excluded from the analysis; for the fits shown in Extended Data Fig. 2k, they were included. Both approaches yielded K_d estimates of the same order, although the fit to the data was much better in the former case. Spectra for Ancα + Ancβ included twinned peaks, which represent caesium iodide adducts on tetramers. For the fits shown in Figs. 1c and 3d, these peaks were excluded; for the fits in Extended Data Fig. 2i, they were included. Both approaches gave almost identical K_d estimates, although the fit to the data was better in the former case.

Hydrogen–deuterium exchange mass spectrometry

All chemicals and reagents were purchased from Sigma Aldrich (Gilligham, UK). Native equilibration buffer contained 100 mM PBS (H_2O), pH 7.4. Labelling buffer contained 100 mM PBS (D_2O), pD 7.4. Quench buffer contained 100 mM potassium phosphate (H_2O), pH 1.9, with 1 M guanadinium chloride. Five microlitres of protein sample was diluted into 55 µl of a deuterated buffer of the same composition and corresponding pD. This resulted in a labelling solution ~92% D_2O. Samples were incubated for between 15 s and 1 h at 20 °C before being quenched with an ice-cold H_2O buffer (pH 1.9) of equal volume. The quenched solution pH was ~2.5 at 0 °C. This was quickly injected into an on-line HDX manager (Waters, Milford, MA, USA). The sample was injected onto a 50-µl sample loop at 0 °C before passing over an immobilized pepsin column (Enzymate Pepsin 5 µm, 2.1 mm × 30 mm, Waters) at 20 °C using an isocratic H_2O (0.1% v/v) formic acid solution (200 µl/min). Peptide products were collected on a trapping column (BEH C18, 1.7 µm, 2.1 mm × 5 mm, Waters) held at 0 °C. After 2 min of collection, and de-salting, peptides were eluted from the trap column on to an analytical column (BEH C18, 1.7 µm, 1 mm × 100 mm, Waters) for separation using a reverse-phase gradient with a flow rate of 40 µl/min. The elution profile using a H_2O/MeCN (+0.1% formic acid v/v) gradient was as follows: 1–7 min 97% water to 65% water, 7–8 min 65% water to 5% water, 8–10 min hold at 5% water. The analytical flow rate was 40 µl/min and the eluate was electrosprayed directly into a Synapt G2Si (Waters, Wilmslow, UK) Q-ToF instrument for mass analysis.

Sample handling was semi-automated using a robotic liquid handling HDX system (LEAP Technologies, Ringwood, Australia) to ensure reproducibility in timings. A blank and cleaning injection cycle was performed between each labelling experiment. Mass spectrometry conditions were as follows: capillary 2.8 kV, sample cone 30 V, source offset 30 V, trap activation 4 V, transfer activation 2 V. The source temperature was set to 80 °C and cone gas flow 80 l/h, the desolvation temperature was 150 °C and the desolvation gas flow was 250 l/h. LeuEnk was used as an internal calibrant and acquired every 30 s. For reference, back-exchange was estimated separately using lyophilized samples of angiotensin II. Angiotensin II was dissolved into D_2O (pH 4.0) and left for 48 h. After that, the sample was loaded onto the same robotic and UPLC system and analysed after 2 min of trapping to give a back-exchange of 31.8 ± 0.2%.

Peptides were identified, in the absence of labelling, by data-independent MS/MS analysis (MS^E) of the eluted peptides and subsequent database searching in the Protein Lynx Global server 3.0 software (Waters). Peptide fragments were generated in the trap region through collisions with Ar gas (0.4 ml/min). Peptide identifications were filtered according to fragmentation quality (minimum fragmentation products per amino acid: 0.2), mass accuracy (maximum [MH]+ error: 5 ppm), and reproducibility (peptides identified in all MS^E repeats) before their integration into HDX analysis. HDX-MS data were processed

in DynamX 3.0 software (Waters), and all automated peptide assignments were manually verified, with noisy and overlapping spectra discarded. External python scripts were written to generate and analyse the Woods plots from data outputs of DynamX.

Sample concentration was varied to control the relative populations of monomeric and dimeric species of Ancα/β. After dilution into the labelling buffer, Ancα/β concentrations were 0.67, 2, 15, and 75 μM; to avoid significant sample overloading of the column when using high concentrations of Ancα/β, samples were diluted during quenching to give an injection quantity of ~15 pmol. To ensure back-exchange occurred equally across all diluted samples, the final ratio of H_2O:D_2O after quenching was kept constant at 54:46 and the pH of the quench buffer adjusted to pH 2.5. This allowed all concentrations to be compared without correcting for back-exchange. All automated peptide assignments were manually verified, with noisy and overlapping spectra discarded. After processing, a sequence coverage of 91% was achieved with a redundancy of 5.3.

Statistical comparison of peptides

For each peptide in the dilution experiment, the difference in deuterium uptake between different conditions was normalized by dividing the difference by the absolute uptake in the dimeric condition (75 μM). In Fig. 2c, peptides that incorporated deuterons in the monomeric condition at quantities statistically indistinguishable from zero ($P < 0.01$) were excluded. For peptide locations and alternative normalization methods, see Extended Data Figs. 6, 7. A permutation test was used to determine whether relative deuterium uptake by residues at IF1 (or IF2) was significantly different from that of other residues. To eliminate statistical non-independence arising from the fact that many peptides overlap, we constructed a non-overlapping peptide set by subsampling without replacement from the total set of peptides, requiring that selected peptides do not share any residues. One thousand such non-overlapping peptide sets were constructed, and a *P* value was estimated for each set using the following permutation test. Peptides in the nonoverlapping set were partitioned into those containing residues mapping to IF1 and those containing no IF1 residues; a similar approach was used to test for a difference between peptides containing IF2 residues and those containing none; peptides containing residues contributing to both interfaces were excluded. The mean of the measured relative uptake difference over peptides in each partition was calculated, and the difference between the means of the two partitions was determined. A null distribution was then estimated by randomly partitioning peptides in the nonoverlapping set into two categories (without changing the size of the categories) and calculating the difference in means between the two randomly permuted peptide partitions. The *P* value was calculated as the proportion of random partitions in which the difference between peptide category means was greater than or equal to that of the difference for the empirical categories. Extended Data Fig. 5 displays the distribution of *P* values calculated in this way for 1,000 non-overlapping peptide sets. An interface category was identified as having significantly increased uptake if the mean *P* value from this analysis was <0.05.

Homology models for Ancα/β IF1 and IF2

Structural modelling of the Ancα/β monomer was performed using SWISS-MODEL. A deoxy structure of an Hbα monomer contained in recombinantly expressed human haemoglobin (1A3N) was used as the template. Hbα was used because its sequence similarity to Ancα/β is greater than that of any other extant globin. Furthermore, both Hbα and Ancα/β form homodimers in isolation, unlike Hbβ (which is a mixture of dimers and tetramers at similar concentrations) or myoglobin. EMBO PISA[62] was used to identify sites in 1A3N subunits that buried >50% of their surface area at the interfaces or formed intersubunit hydrogen-bonding or salt bridge contacts at either IF1 or IF2. The HADDOCK 2.2 webserver was used to dock two Ancα/β monomers along an IF1 or an IF2 orientation by specifying the corresponding homologous residues (1a3n). The best scoring docked complex was used for all subsequent analyses and visualizations.

Homology models, interface burial, and contact maps for Ancα + Ancβ and Ancα/β14

Structural modelling was performed using SWISS-MODEL. A deoxy structure of recombinantly expressed human haemoglobin (PDB 1A3N) was used as the template for Ancα + Ancβ and for Ancα/β14 + Ancα. The extant Hbα and Hbβ were used as templates because they have higher sequence identity to to Ancα and Ancα/β14, respectively, than any other globin paralogues. EMBO PISA was used to estimate residue burial at the interfaces and to predict hydrogen bonds across interfaces. Residues were classified as contributing to an interface if their solvent-accessible surface area was reduced by >10% in the assembled form relative to the nonassembled form. Van der waals contacts were identified as pairs of cross-interface atoms with centre-to-centre distances <3.5 Å, using a custom script. PyMOL v4.19 was used to visualize and render protein structures. The similarity between interfaces in the homology model and those in X-ray crystal structures of extant haemoglobins was assessed by aligning the Ancα/β14 + Ancα tetramer to Hb from human (1A3N) and rainbow trout (*Oncorhynchus mykiss* 2R1H) (Extended Data Fig. 10).

Reporting summary

Further information on research design is available in the Nature Research Reporting Summary linked to this paper.

Data availability

Reconstructed ancestral sequences have been deposited in GenBank (IDs MT079112, MT079113, MT079114, MT079115). Alignment and inferred phylogeny, raw mass spectra, oxygen-binding data, and homology model coordinates have been deposited at https://doi.org/10.5061/dryad.w0vt4b8mx. HDX-MS data are available at https://doi.org/10.5287/bodleian:5zRrdMB7E.

Code availability

Scripts for analysis for the HDX permutation analysis and identification of contacts between subunits in modelled structures have been deposited at https://github.com/JoeThorntonLab/Hemoglobin-evolution.

40. Katoh, K., Rozewicki, J. & Yamada, K. D. MAFFT online service: multiple sequence alignment, interactive sequence choice and visualization. *Brief. Bioinform.* **20**, 1160–1166 (2019).
41. Guindon, S. et al. New algorithms and methods to estimate maximum-likelihood phylogenies: assessing the performance of PhyML 3.0. *Syst. Biol.* **59**, 307–321 (2010).
42. Le, S. Q. & Gascuel, O. An improved general amino acid replacement matrix. *Mol. Biol. Evol.* **25**, 1307–1320 (2008).
43. Anisimova, M. & Gascuel, O. Approximate likelihood-ratio test for branches: A fast, accurate, and powerful alternative. *Syst. Biol.* **55**, 539–552 (2006).
44. Anisimova, M., Gil, M., Dufayard, J. F., Dessimoz, C. & Gascuel, O. Survey of branch support methods demonstrates accuracy, power, and robustness of fast likelihood-based approximation schemes. *Syst. Biol.* **60**, 685–699 (2011).
45. Hoffmann, F. G. et al. Evolution of the globin gene family in deuterostomes: lineage-specific patterns of diversification and attrition. *Mol. Biol. Evol.* **29**, 1735–1745 (2012).
46. Hoffman, F. G. & Storz, J. F. The α^D-globin gene originated via duplication of an embryonic α-like globin gene in the ancestor of tetrapod vertebrates. *Mol. Biol. Evol.* **24**, 1982–1990 (2007).
47. Yang, Z. PAML 4: phylogenetic analysis by maximum likelihood. *Mol. Biol. Evol.* **24**, 1586–1591 (2007).
48. Schwarze, K., Singh, A. & Burmester, T. The full globin repertoire of turtles provides insights into vertebrate globin evolution and functions. *Genome Biol. Evol.* **7**, 1896–1913 (2015).
49. Natarajan, C. et al. Expression and purification of recombinant hemoglobin in *Escherichia coli*. *PLoS ONE* **6**, e20176 (2011).
50. Imai, K. *Allosteric Effects in Haemoglobin* (Cambridge Univ. Press, 1982).
51. Bonaventura, C. & Bonaventura, J. Anionic control of function in vertebrate hemoglobins. *Integr. Comp. Biol.* **20**, 131–138 (1980).
52. Weber, R. E. & Jensen, F. B. Functional adaptations in hemoglobins from ectothermic vertebrates. *Annu. Rev. Physiol.* **50**, 161–179 (1988).

53. Isaacks, R. E. & Harkness, D. R. Erythrocyte organic phosphates and hemoglobin function in birds, reptiles, and fishes. *Integr. Comp. Biol.* **20**, 115–129 (1980).
54. Benesch, R., Benesch, R. E. & Enoki, Y. The interaction of hemoglobin and its subunits with 2,3-diphosphoglycerate. *Proc. Natl Acad. Sci. USA* **61**, 1102–1106 (1968).
55. Imaizumi, K., Imai, K. & Tyuma, I. The linkage between the four-step binding of oxygen and the binding of heterotropic anionic ligands in hemoglobin. *J. Biochem.* **86**, 1829–1840 (1979).
56. Grispo, M. T. et al. Gene duplication and the evolution of hemoglobin isoform differentiation in birds. *J. Biol. Chem.* **287**, 37647–37658 (2012).
57. Richard, V., Dodson, G. G. & Mauguen, Y. Human deoxyhaemoglobin-2,3-diphosphoglycerate complex low-salt structure at 2.5 A resolution. *J. Mol. Biol.* **233**, 270–274 (1993).
58. Arnone, A. X-ray diffraction study of binding of 2,3-diphosphoglycerate to human deoxyhaemoglobin. *Nature* **237**, 146–149 (1972).
59. Arnone, A. P. M. Structure of inositol hexaphosphate–human deoxyhaemoglobin complex. *Nature* **249**, 195–197 (1974).
60. Cong, X. et al. Determining membrane protein-lipid binding thermodynamics using native mass spectrometry. *J. Am. Chem. Soc.* **138**, 4346–4349 (2016).
61. Marty, M. T. et al. Bayesian deconvolution of mass and ion mobility spectra: from binary interactions to polydisperse ensembles. *Anal. Chem.* **87**, 4370–4376 (2015).
62. Krissinel, E. & Henrick, K. Inference of macromolecular assemblies from crystalline state. *J. Mol. Biol.* **372**, 774–797 (2007).

Acknowledgements We thank C. Natarajan for technical advice and the Hb co-expression plasmid and members of the Thornton laboratory for technical advice and comments on the manuscript. Supported by NIH R01-GM131128 and R01-GM121931 (J.W.T.), NIH R01-HL087216 and NSF OIA-1736249 (J.F.S.), NIH T32-GM007197 (C.R.C.-R.), a Chicago Fellowship (G.K.A.H.), BBSRC BB/L017067/1 and Waters Corp. (J.L.P.B.).

Author contributions A.S.P. identified and developed the model system. A.S.P., G.K.A.H., and J.W.T. coordinated the project, interpreted the data, and led writing of the manuscript. A.S.P. performed and interpreted phylogenetic analyses and biochemical assays. A.V.S. and J.F.S. performed and interpreted oxygen binding assays. Y.L. and A.L. performed and interpreted native mass spectrometry experiments. S.A.C. and J.L.P.B. performed and interpreted HDX experiments. C.R.C.-R. performed and interpreted biochemical assays. All authors contributed to writing the manuscript.

Competing interests The authors declare no competing interests.

Additional information

Supplementary information is available for this paper at https://doi.org/10.1038/s41586-020-2292-y.

Correspondence and requests for materials should be addressed to J.W.T.

Peer review information *Nature* thanks Nobuhiko Tokuriki and the other, anonymous, reviewer(s) for their contribution to the peer review of this work.

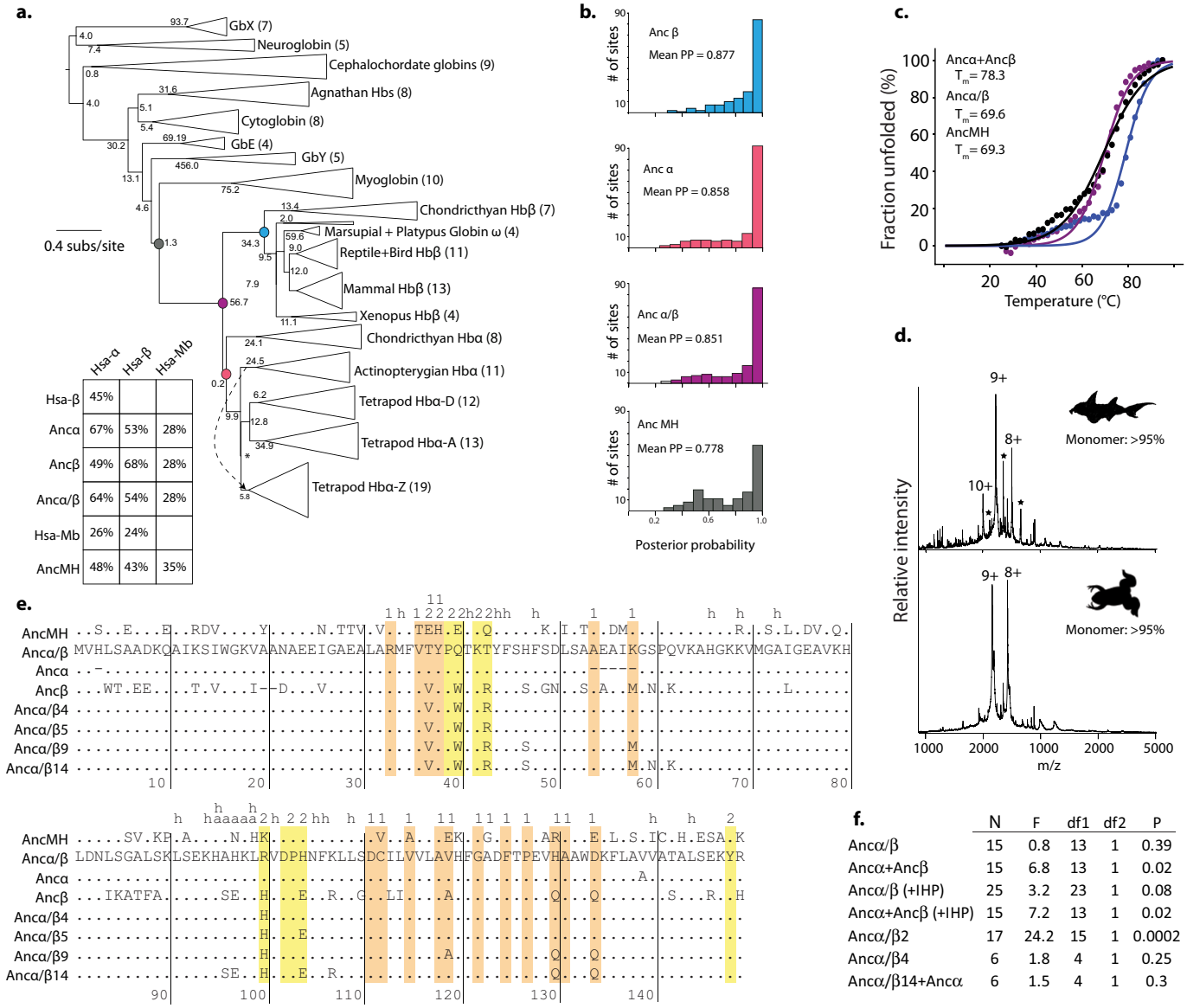

	N	F	df1	df2	P
Ancα/β	15	0.8	13	1	0.39
Ancα+Ancβ	15	6.8	13	1	0.02
Ancα/β (+IHP)	25	3.2	23	1	0.08
Ancα+Ancβ (+IHP)	15	7.2	13	1	0.02
Ancα/β2	17	24.2	15	1	0.0002
Ancα/β4	6	1.8	4	1	0.25
Ancα/β14+Ancα	6	1.5	4	1	0.3

Extended Data Fig. 1 | Reconstruction of ancestral haemoglobin and precursors. a, Phylogeny of Hb and related globins. Node supports are shown as approximate likelihood ratio statistic[59,60]. The number of sequences in each group is shown in parentheses. Ancestral sequences reconstructed in this study are shown as coloured circles. Arrow, branch swap that differentiates this phylogeny from the unconstrained ML phylogeny, which requires additional gene gains and losses. The tree is rooted on neuroglobin and globin X, paralogues that duplicated before the divergence of deuterostomes and protostomes[61]. Inset, pairwise sequence identities among extant (human, Hsa) and reconstructed ancestral globins. **b**, Distribution across sites of the posterior probabilities (PP) of maximum a posteriori states for reconstructed ancestral proteins. **c**, Thermal stability of ancestral globins. Points, fraction of secondary structure lost as temperature increases in Ancα/β (purple), Ancα + Ancβ (blue) and AncMH (black), measured by circular dichroism spectroscopy at 222 nm, relative to signal at 23 °C. T_m and its s.e. were estimated by nonlinear regression; the best-fit curve (lines) are shown. Each point is the mean of four measurements. **d**, Native mass spectra of globin Y from elephant shark (top, *Callorhinchus milii*) and African clawed frog (bottom, *X. laevis*) at 30 μM. Charge states of haem-bound monomer shown. Asterisk, cleavage products. Spectra were collected once. **e**, Sequence alignment of reconstructed ancestral globins. Dots, states identical to Ancα/β; yellow, IF2 sites; orange, IF1 sites; h, sites 4 Å away from the haem; a, sites that link the haem-coordinated proximal histidine (H95) to IF2. **f**, Statistical test of cooperativity of oxygen binding for ancestral proteins and mutants. An *F*-test was used to compare the fit of a model in which the Hill coefficient (n) is a free parameter to a null model with no cooperativity ($n = 1$). Computed *P* value and degrees of freedom (df) are shown. *N*, number of concentrations measured. $^*P < 0.05$. Data were pooled across replicate experiments for nonlinear regression.

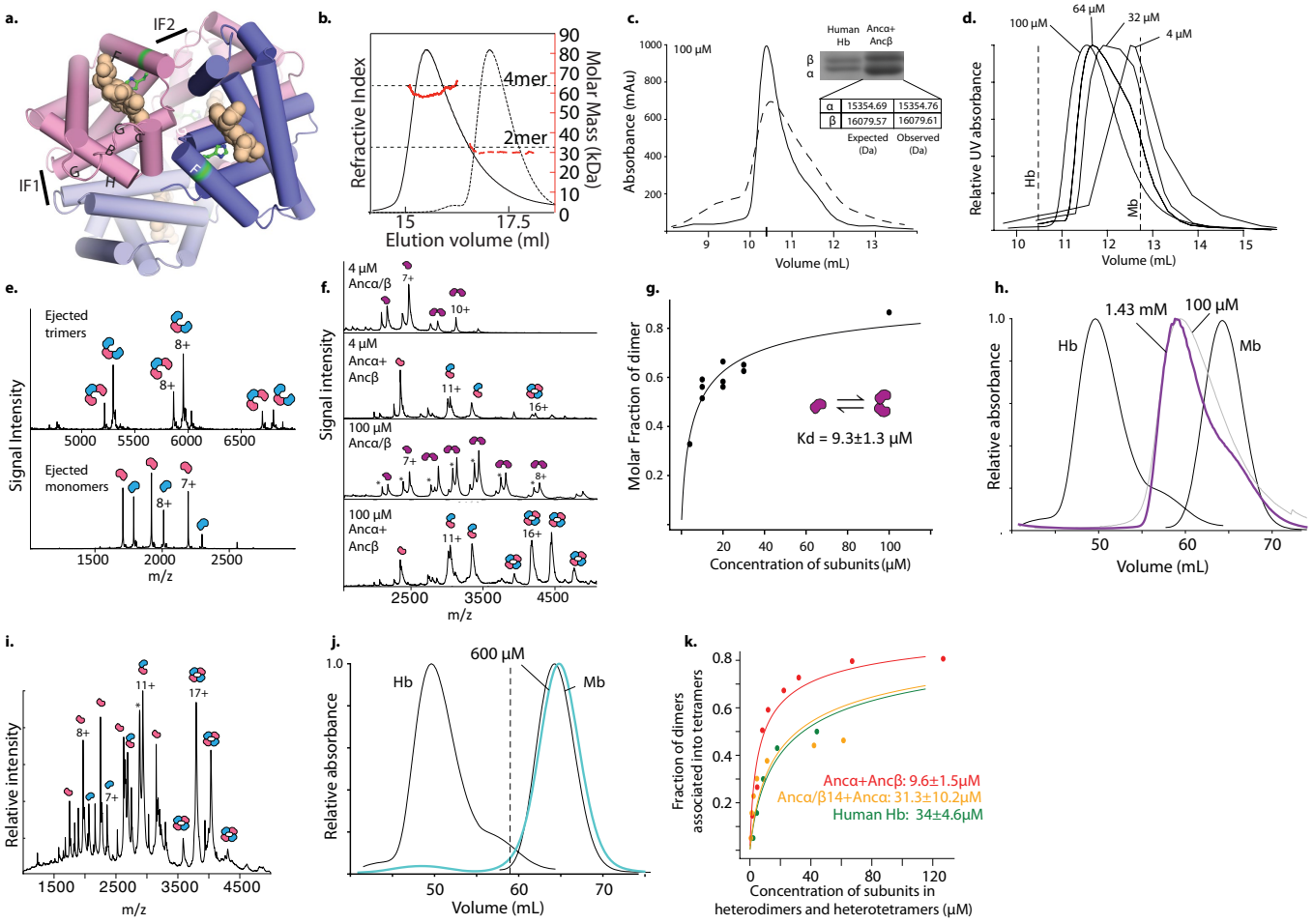

Extended Data Fig. 2 | Stoichiometric characterization of ancestral globin complexes. a, Homology model of Ancα + Ancβ (template 1A3N) showing haem (tan spheres). Blue cartoon, Ancβ subunits; red, Ancα. Helices and interfaces are labelled. Green, proximal histidine. **b**, SEC and multiangle light scattering of Ancα/β (90 µM) and Ancα + Ancβ (60 µM). Black, relative refractive index; red, estimated molar mass. Dashed lines, Ancα/β; solid lines, Ancα+Ancβ. Dashed horizontal lines, expected mass for dimers and tetramers. **c**, SEC of human Hb (dashed) and Ancα + Ancβ (solid) at 100 µM. Top inset, SDS–PAGE of these complexes, with bands corresponding to α- and β-subunits. Bottom inset, masses estimated by denaturing MS of Ancα + Ancβ, compared to expected masses based on primary sequence. **d**, SEC of Ancα/β across a series of concentrations. Dashed vertical lines, elution peak volumes of human haemoglobin tetramer and myoglobin monomer. **e**, Tandem MS of the heterotetrameric peak in the Ancα + Ancβ nMS (indicated in Fig. 1b). Ejected monomer and trimer charge series and the subunits they contain are shown. Pink, Ancα; blue, Ancβ. **f**, nMS of Ancα + Ancβ and Ancα/β at 4 µM and 100 µM. Charge series and fitted stoichiometries are indicated. *Unhaemed apo form. **g**, Monomer–dimer association by Ancα/β. Abundances of monomers and dimers were characterized using nMS across a range of concentrations. Circles, fraction of all subunits that were assembled into dimers as a function of the concentration of subunits in all states. Nonlinear regression (line) was used to estimate the dissociation constant (K_d, with s.e.). **h**, SEC of Ancα/β at high concentrations (purple and grey lines). Black curves show SEC traces of human Hb and myoglobin for comparison. **i**, nMS of human Hb at 50 µM. **j**, SEC of AncMH (cyan) at a high concentration. SEC traces of human Hb and myoglobin (black) are shown for reference. Dashed line, Ancα/β dimer elution peak volume (see **f**). **k**, Alternative estimation of affinity of dimer–tetramer association by nMS. For human Hb (green) and Ancα/β14 + Ancα (orange), the fraction of heterodimers incorporated into heterotetramers includes both haem-deficient and holo-heterodimers. For Ancα + Ancβ (red), caesium iodide adduct was included. Compare to Figs. 1d and 3d. K_d values (with s.e.) were estimated by nonlinear regression (lines). All concentrations are expressed in terms of monomer. All nMS and SEC experiments were performed once at each concentration.

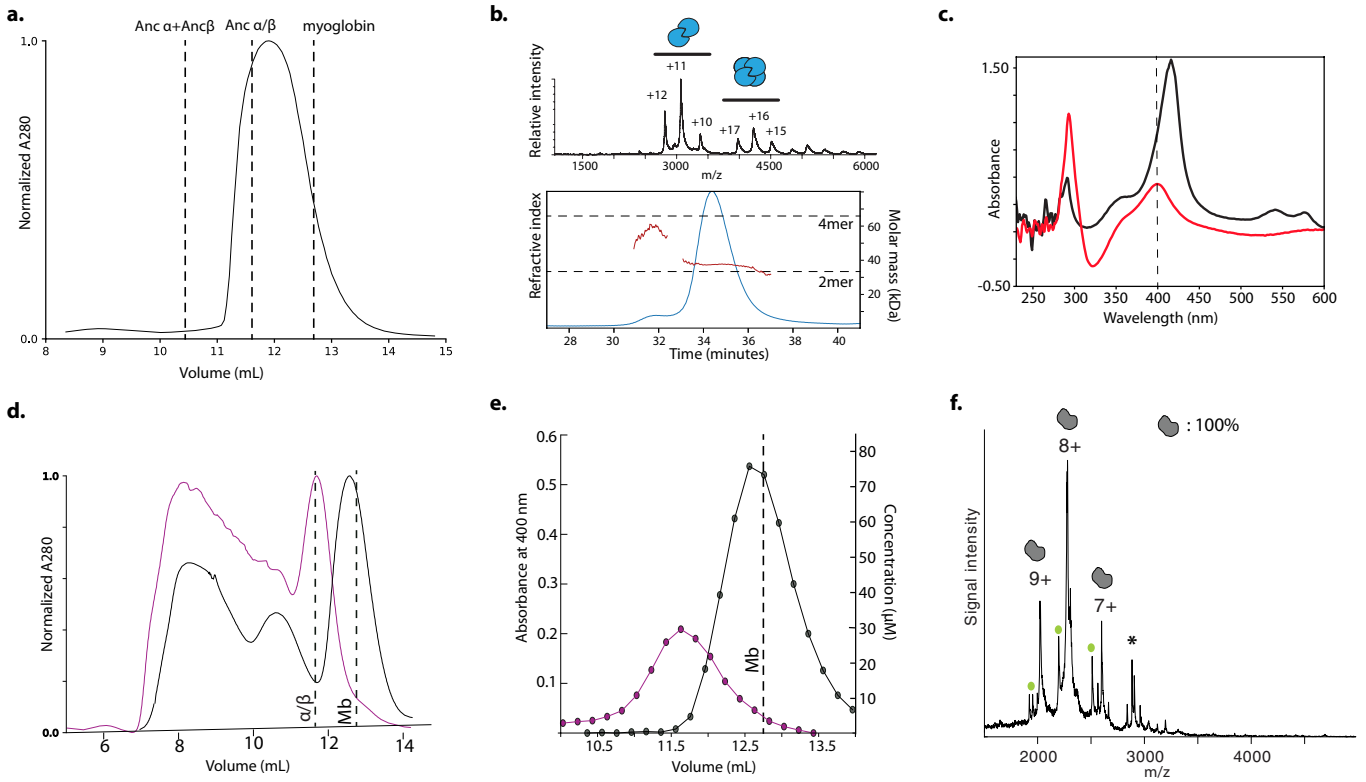

Extended Data Fig. 3 | Stoichiometric analysis of Ancα, Ancβ, and AncMH. **a**, SEC of Ancα at 75 μM. **b**, nMS spectrum (top, at 20 μM) and SEC–MALS (bottom) of Ancβ. Blue, UV absorption; red, molar mass estimated by light scattering. **c**, Colorimetric haemoglobin concentration assay. Absorbance spectra before (black) and after (red) adding 150 μl Triton/NaOH reagent to 50 μl purified Ancα/β. In the presence of reagent, globins absorb at 400 nm. **d**, SEC of crude cell lysate after expression of AncMH (purple) and Ancα/β (black). Dashed lines, expected elution volumes for monomer (human myoglobin) and dimer (Ancα/β). **e**, Colorimetric haemoglobin concentration assay on collected SEC fractions of crude lysate containing AncMH (purple) and Ancα/β (black). **f**, nMS of His-tagged AncMH at 70 μM, with monomer charge series indicated. *Cleavage product. Green, apo. Fractional occupancy of the monomeric form is shown. All experiments were performed once.

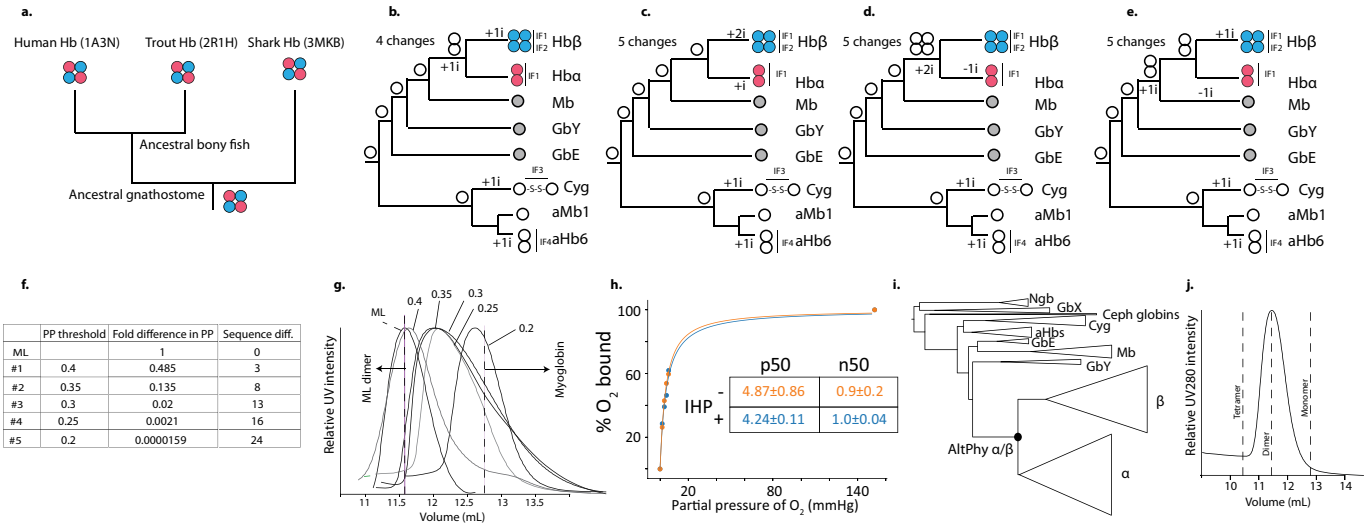

	PP threshold	Fold difference in PP	Sequence diff.
ML		1	0
#1	0.4	0.485	3
#2	0.35	0.135	8
#3	0.3	0.02	13
#4	0.25	0.0021	16
#5	0.2	0.0000159	24

Extended Data Fig. 4 | Biochemical inferences about ancestral Hbs are robust to uncertainty in sequence reconstructions. a–**e**, Maximum parsimony inferences of ancestral stoichiometry and interface losses or gains based on the distribution of stoichiometries among extant globins. **a**, Hbs in all extant lineages of jawed vertebrates are heterotetramers, supporting the inference that AncHb was heterotetrameric. Stoichiometries from representative species' Hbs are shown with PDB IDs. **b**–**e**, Each panel shows a hypothetical set of ancestral stoichiometries, plotted on the phylogeny of extant Hb subunits and closely related globins, with the minimal number of changes required by each scenario. **b**, The most parsimonious reconstruction is that Ancα/β was a homodimer and AncMH was a monomer. **c**, For Ancα/β to have been a tetramer, early gain and subsequent loss of IF2 in Hbα would be required. **d**, For Ancα/β to have been a monomer, IF1 would have to have been independently gained in Hbα and Hbβ. **e**, For AncMH to have been a dimer, IF1 would have to have been lost in lineages leading to the monomers myoglobin (Mb) and globin E (GbE)[12,13]. The dimeric globins most closely related to Hb—agnathan 'haemoglobin' (aHb) and cytoglobin (Cyg)—use interfaces that are structurally distinct from those in Hb[15,16], indicating independent acquisition. **f**–**j**, Alternative reconstructions of Ancα/β are biochemically similar to the ML reconstruction. **f**, Alternative ancestral versions of Ancα/β were constructed, each containing the the ML state at every unambiguously reconstructed site and the second most likely state at all ambiguously reconstructed sites, using different thresholds of ambiguity. For each alternative reconstruction, the table shows the threshold posterior probability (PP) used to define an ambiguous site, as well as the fold-difference in total PP of the entire sequence and the number of sites that differ from the ML reconstruction. **g**, SEC at 75 μM of ML reconstruction of Ancα/β and AltAll reconstructions, which contain all plausible alternative states with PP above a threshold. Dashed lines show elution peak volumes for the dimeric ML α/β and monomeric human myoglobin. Constructs that elute between the expected volumes for dimer and monomer indicate dimers that partially dissociate during the run. None tetramerize; all form predominantly dimers, except AltAll(PP >0.2), which is ~62,000 times less probable than ML, which is mostly monomeric. UV traces were collected once for each construct. **h**, Oxygen binding curves of Ancα/β-AltAll(0.25), the dimeric AltAll with the lowest PP, with and without 2× IHP. Dissociation constant (P50, with s.e.) estimated by nonlinear regression is shown. Lack of cooperativity is indicated by the Hill coefficient (n50 = ~1.0). Oxygen binding at each concentration was measured once. **i**, Alternate globin phylogeny that is more parsimonious than the ML topology with respect to gene duplications and synteny but has a lower likelihood given the sequence data. A version of Ancα/β (Ancα/β-AltPhy) was reconstructed on this phylogeny. **j**, SEC of Ancα/β-AltPhy. Dashed lines show expected elution volumes for various stoichiometric forms.

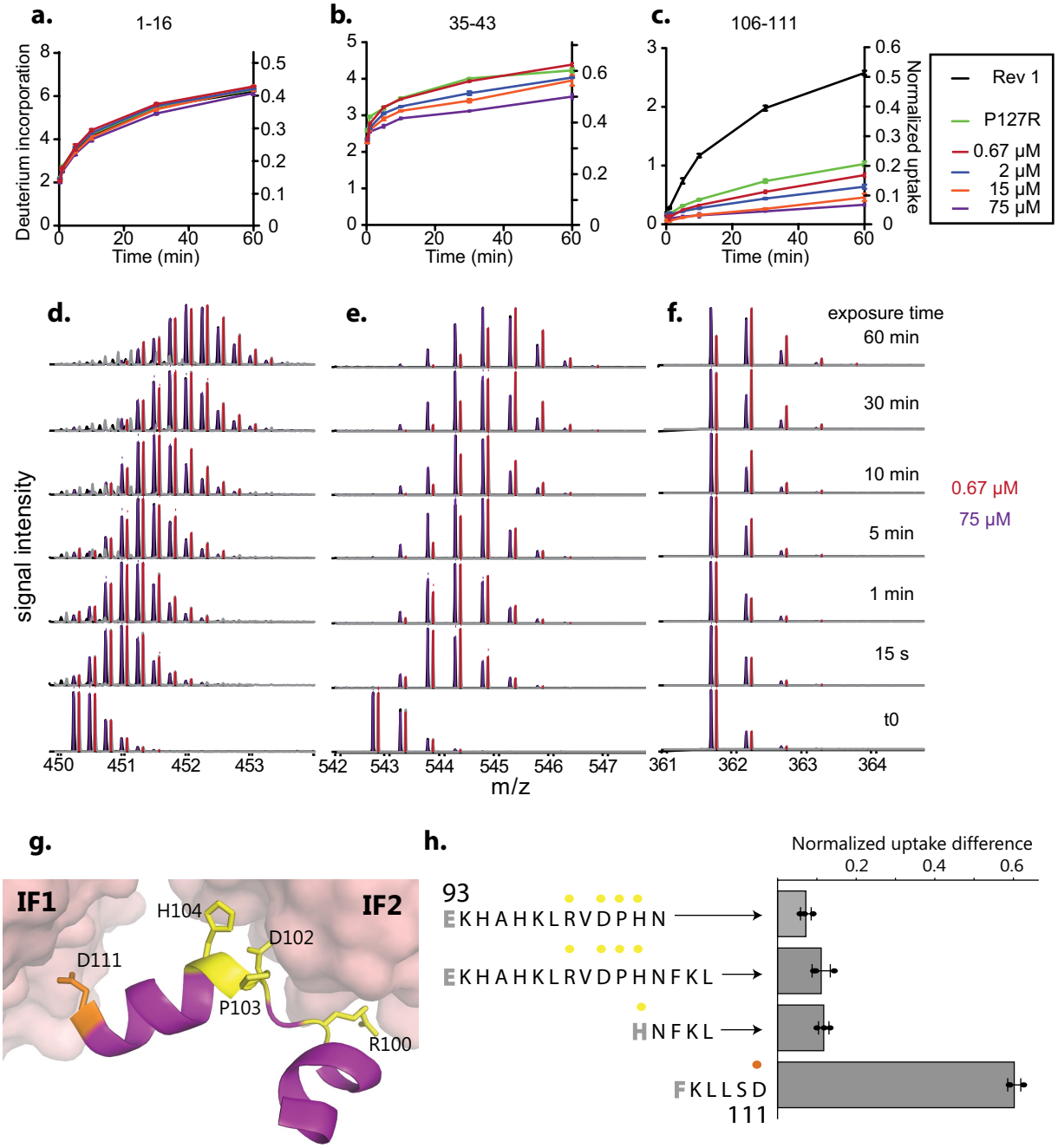

Extended Data Fig. 5 | HDX-MS of Ancα/β. a–**c**, Deuterium uptake measurements across time for three peptides. Left vertical axis, raw deuterium incorporation; right vertical axis, deuterium incorporation divided by the total number of exchangeable amide hydrogens per peptide. Uptake curves for four concentrations of mutants IF1rev and P127R are shown. Each point shows mean ± s.e. of three replicate measurements. **d**–**f**, Raw MS spectra for the peptides shown in **a**–**c**, respectively, at 0.67 μM (red, at which the protein is monomeric), and 75 μM (purple, at which it is entirely dimeric: see Extended Data Fig. 2). The traces are slightly offset to allow visualization. One replicate at each incubation time is shown. **g**, Amino acids 99 to 111 contact IF1 (orange) or IF2 (yellow). The homology model of one chain of Ancα/β (cartoon and sticks) was aligned to the α-subunit of human Hb (PDB 1A3N); β-subunits are shown as surfaces. **h**, Normalized deuterium uptake difference (mean ± s.e. from three replicates), defined as the uptake difference between monomer and dimer divided by the uptake of the monomer, observed for peptides containing amino acids 99–111. Grey N-terminal residues do not contribute to uptake. Amino acid sequences are aligned and labelled (orange dots, IF1; yellow dots, IF2).

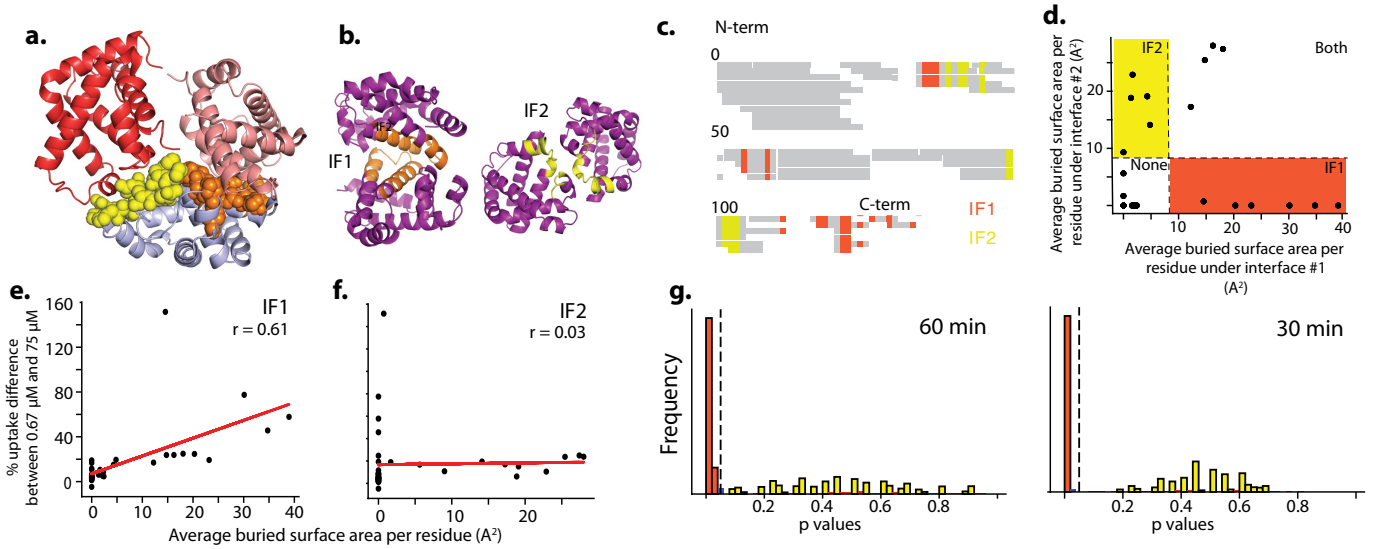

Extended Data Fig. 6 | Statistical analysis of HDX-MS results for peptides containing interface residues. a, Residues in human Hb (PDB 1A3N) that bury at least 50% of their surface area in either IF1 (orange) or IF2 (yellow) are shown as spheres. Red and pink, α-subunits; blue, β-subunits. **b**, Homology models of Ancα/β dimer across IF1 (left) and IF2 (right). Two subunits of Ancα/β were computationally docked using HADDOCK using the α1/β1 interface (IF1, left) or α1/β2 interface (IF2, right) of human Hb (1A3N) as a template. **c**, Coverage of peptides produced by trypsinization of Ancα/β, assessed by MS. Orange and yellow, sites that bury surface area at IF1 and IF2 in the modelled dimeric structures, respectively. **d**, Classification of trypsin-produced peptides that contribute to IF1 or IF2. Each circle represents one peptide, plotted by average surface area per residue buried at each interface (total buried area divided by total number of residues). Dashed lines, cutoffs to classify peptides as contributing to IF1 (orange) or IF2 (yellow). **e**, **f**, Correlation between change in deuterium uptake and burial of surface area at IF1 or IF2. Each point is one of 47 peptides, plotted according to the normalized difference in deuterium uptake between concentrations at which monomer or dimer predominates (0.67 or 75 μM, normalized by uptake at 75 μM) and average buried surface area at IF1 or IF2. *r*, Pearson correlation coefficient. **g**, Permutation test to evaluate the difference in deuterium uptake at two time points by peptides containing IF1 versus all other peptides (orange), or IF2 versus all other peptides (yellow). To avoid non-independence, the experimental data were reduced to a set of nonoverlapping peptides by sampling without replacement. Peptides were categorized by whether they contained residues at IF1, IF2, or neither; peptides that contributed to both IFs were excluded. For each interface, the mean uptake by peptides contributing to the interface was calculated, as was the mean uptake by peptides not in that category, and the difference in means was recorded. Peptide assignment to categories was then randomized, and the difference in mean uptake recorded; this permutation process was repeated until all possible randomized assignment schemes for those peptides had been sampled once. *P* value, fraction of permuted assignment schemes with a difference in mean uptake between categories greater than or equal to that from the true scheme. This process was repeated for 1,000 nonoverlapping peptide sets; the histogram shows the frequency of *P* values across these sets. Dashed line, $P = 0.05$.

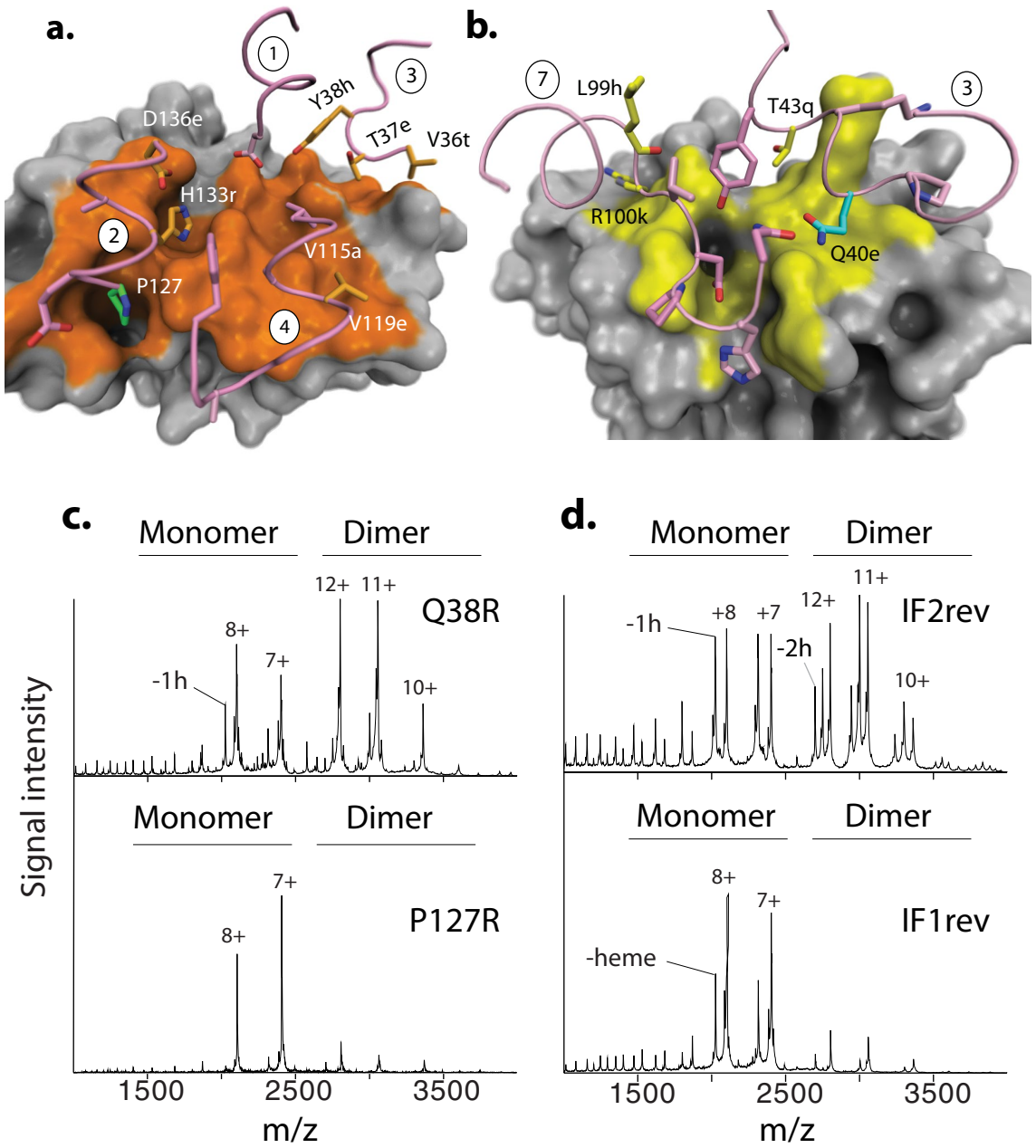

Extended Data Fig. 7 | Dissection of IF1 and IF2 by HDX-MS and mutagenesis. a, **b**, Peptides with residues contributing to IF1 (**a**) or IF2 (**b**) that have the largest relative uptake difference upon dimerization are shown as purple tubes. Sticks, side chains predicted to contact the other subunit (orange surface, IF1; yellow surface, IF2). Side chains are coloured orange (IF1) or yellow (IF2) if they were substituted between AncMH and Ancα/β; purple, unchanged in that interval; green, site for targeted mutation P127; blue, Q40. Circled numbers show the rank of each peptide among all peptides for the normalized difference in deuterium uptake between monomer and dimer conditions. Homology models of the Ancα/β dimer using half-tetramers of human Hb (1A3N) are shown. In **a**, the dimer is modelled using the α1/β1 subunits; in **b**, it is modelled on the α1/β2 subunits. **c**, **d**, nMS of interface mutants Q40R (at IF2) and P127R (at IF1) and for mutants IF1rev and IF2rev, in which interface residues in Ancα/β were reverted to their states in AncMH. All assays at 20 μM. Stoichiometries and charge states are labelled. Unhaemed peak series due to haem ejection during nMS is labelled. Spectra were collected once.

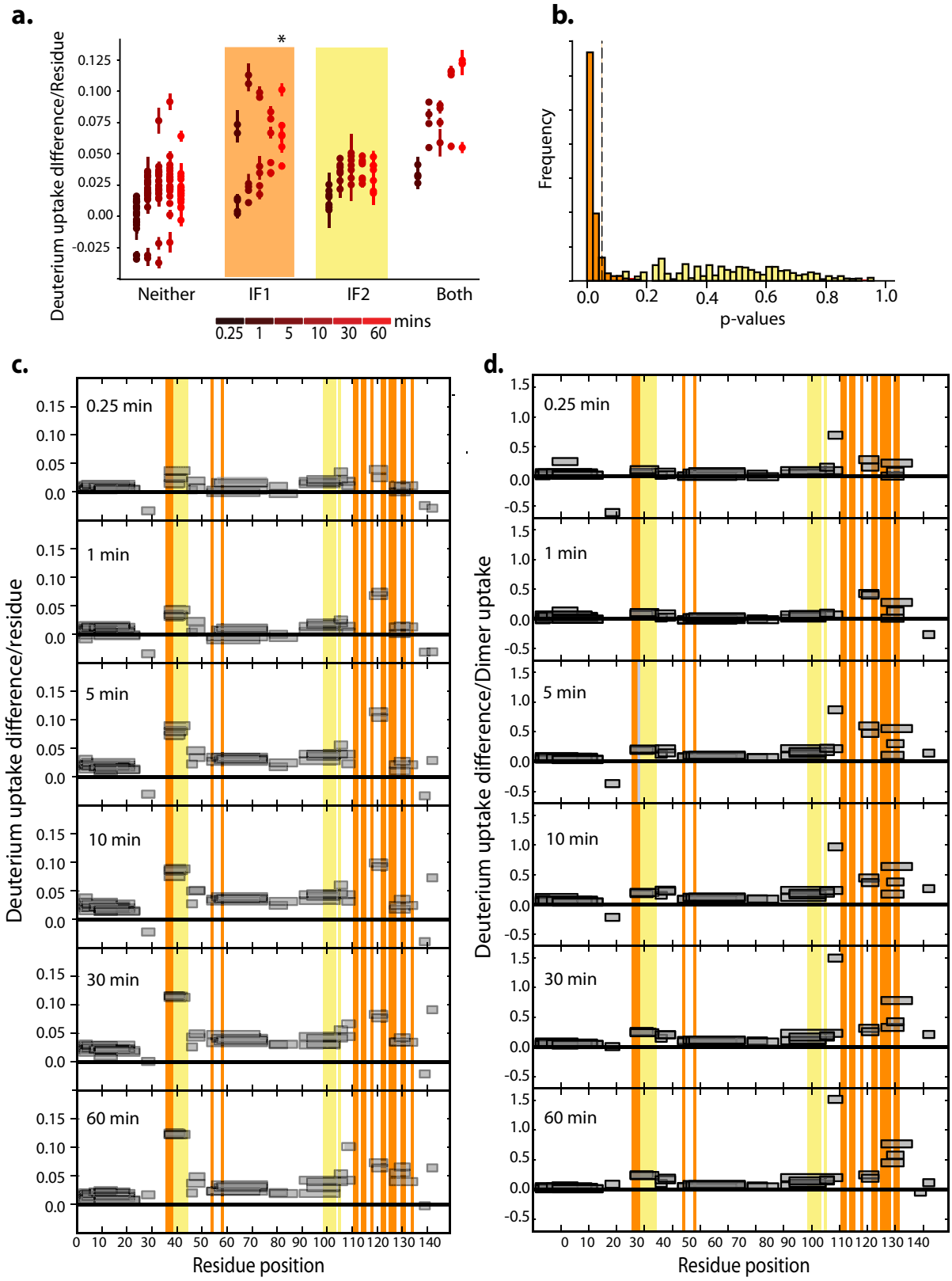

Extended Data Fig. 8 | See next page for caption.

Extended Data Fig. 8 | Alternative methods to normalize deuterium uptake. a, Deuterium uptake difference between monomer (0.67 μM) and dimer (75 μM) at each time point was normalized by the length of each peptide. Peptides were categorized by the interface to which they contribute, as in Fig. 2c. *Interface peptide sets that show significantly increased uptake upon dilution when compared to peptides outside of that interface, as determined by a permutation test (see Extended Data Fig. 6). Each point shows the mean ± s.e. from three replicates. **b**, Permutation test to evaluate the difference in deuterium uptake at 60 min by peptides at each interface, when uptake difference per peptide is normalized by length (as described in Extended Data Fig. 6g). Orange, peptides with IF1-containing residues versus those with no IF1 residues. Yellow, IF2-containing peptides versus those with no IF2 residues. Dashed line, $P = 0.05$. **c**, **d**, Average deuterium uptake difference per residue (**c**) and uptake difference normalized by dimer uptake (**d**) for peptides at different time points. Orange, IF1 sites; yellow, IF2 sites. Each rectangle shows the position of the peptide in the linear sequence and its uptake (mean of three replicates).

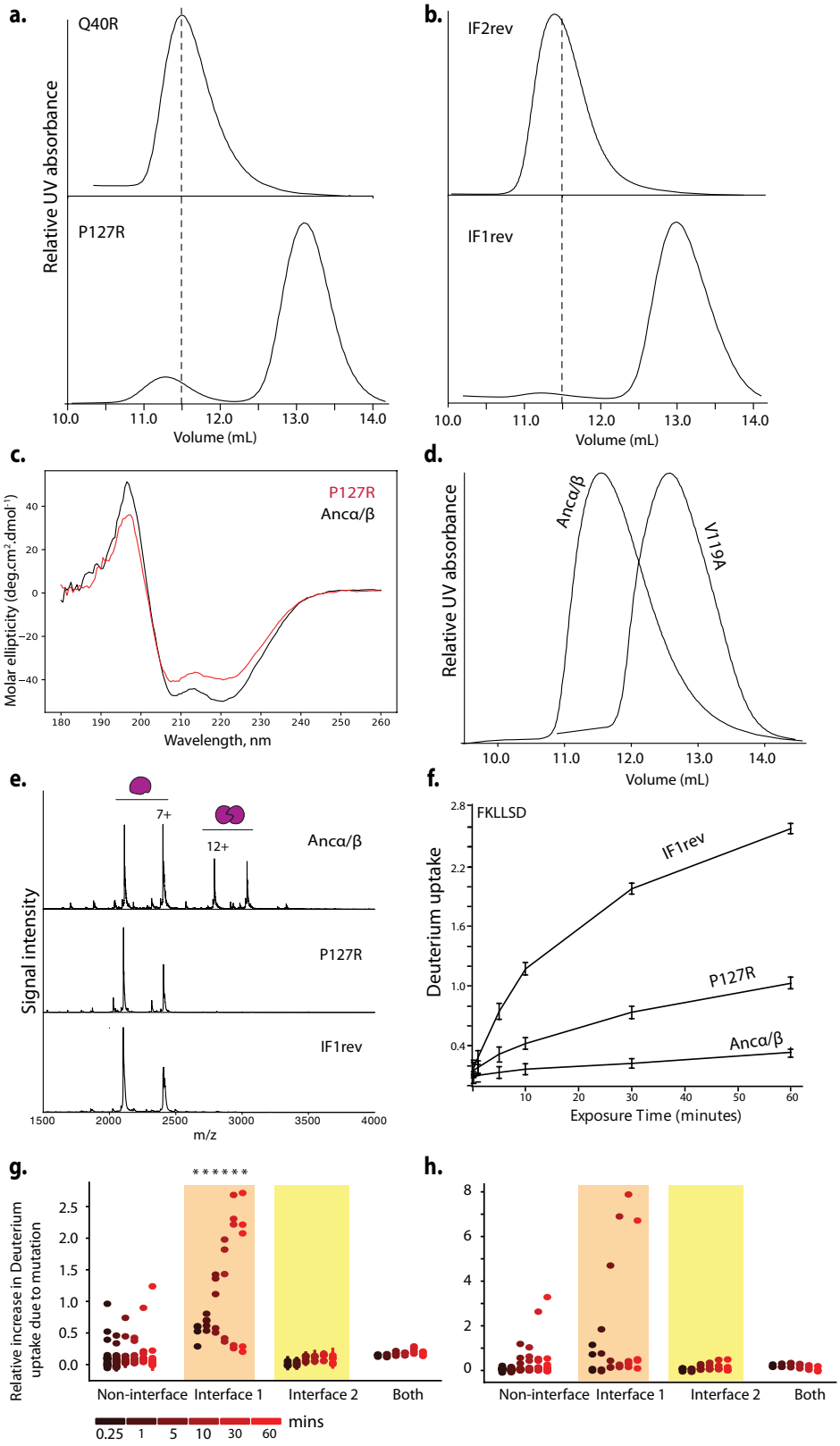

Extended Data Fig. 9 | See next page for caption.

Extended Data Fig. 9 | Effect of interface-disrupting mutations on Ancα/β. **a**, **b**, SEC of mutants at IF2 (Q40R and IF2rev, which reverts all substitutions that occurred between AncMH and Ancα/β at IF2 sites) and at IF1 (P127R and IF1rev) at 100 μM. Dashed line, elution peak volume for Ancα/β. **c**, Circular dichroism spectra for P127R and Ancα/β, showing comparable helical structure. **d**, SEC from IF1 mutant V119A at 64 μM, compared to Ancα/β. **e**, nMS of Ancα/β, P127R and IF1rev at 10 μM. Stoichiometries and charges are shown. For **a**–**d**, nMS and SEC experiments were performed once per concentration. **f**, Normalized deuterium uptake by IF1-containing peptide 106–111 in HDX-MS of Ancα/β (75 μM) and mutants P127R (2 μM) and IF1rev (2 μM). Mean ± s.e. of three replicates. **g**, **h**, Difference between deuterium uptake by each peptide in Ancα/β and uptake by the same peptide in IF1 mutants P127R (**g**) and IF1rev (**h**), both at 2 μM, normalized by uptake in Ancα/β. Peptides are classified by interface category. Mean ± s.e. of three replicates. *Peptide sets that have significantly increased relative uptake (by permutation test, see Extended Data Fig. 6) compared to all other peptides (peptides containing both IF1 and IF2 residues excluded).

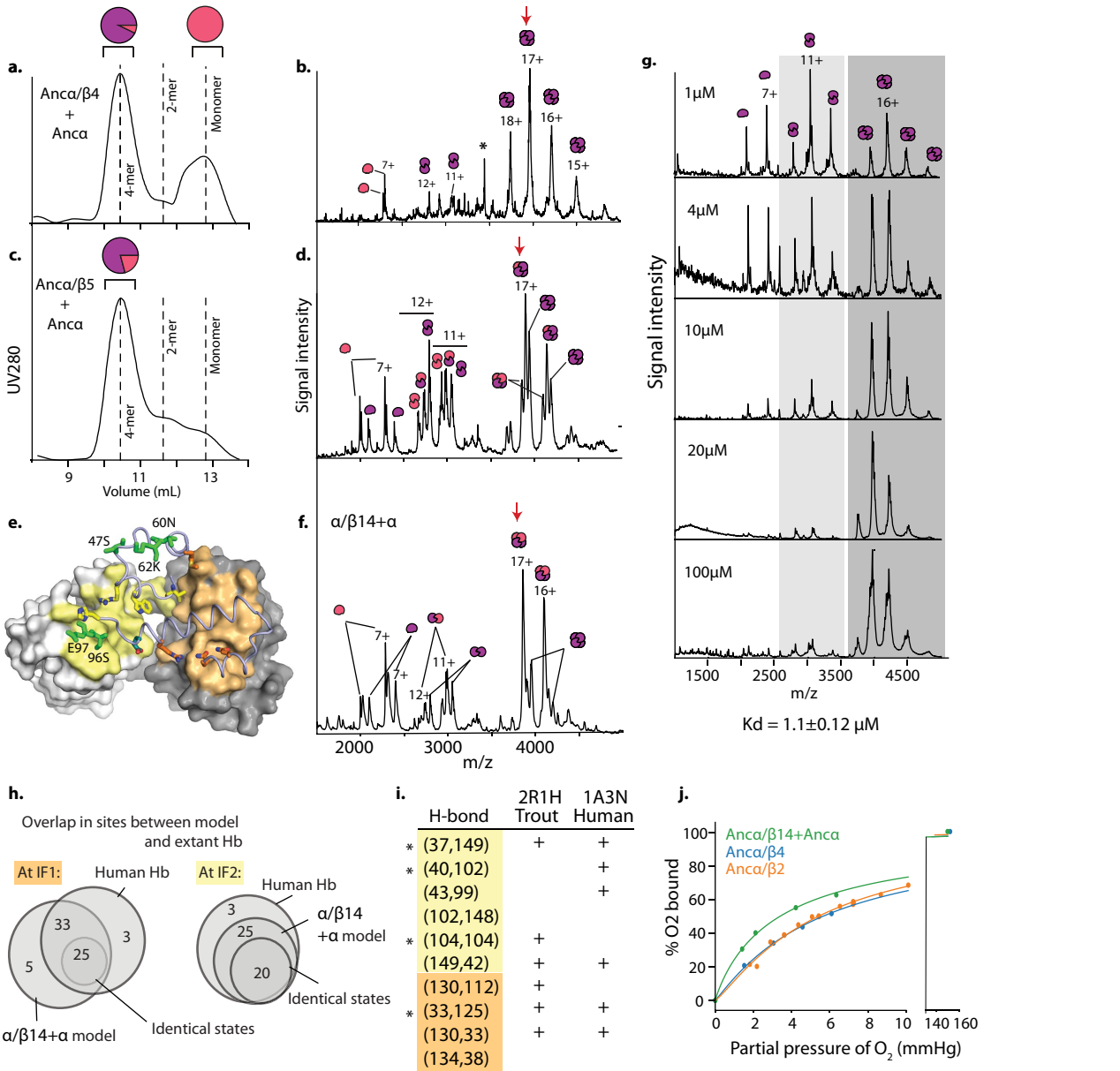

Extended Data Fig. 10 | Genetic mechanisms of tetramer evolution. a, **c**, SEC of Ancα/β containing sets of historical substitutions, when coexpressed and purified with Ancα. Dashed lines, elution volumes of known stoichiometries (4-mer, Ancα + Ancβ; 2-mer, Ancα/β; monomer, human myoglobin). Pie charts, relative proportions of α (pink) and α/β mutant (purple) subunits in fractions corresponding to each peak, as determined by high-resolution MS (Extended Data Fig. 11). **b**, nMS of tetrameric fraction in **a** at 20 μM (monomer concentration). *Apparent impurity. Together, **a** and **b** show that tetramers formed by coexpression of Ancα/β4 + Ancα incorporate virtually no α-subunits. Occupancy from this experiment is shown in Fig. 3b. **d**, **f**, nMS of unfractionated purified protein complexes of Ancα/β5 + α and Ancα/β14 + α at 20 μM. Charge series, stoichiometries indicated. Red arrows, peaks isolated for further characterization by tandem MS (Extended Data Fig. 11). **e**, Homology model of Ancα/β14 + α using Human Hb (1A3N) as template. Yellow and cyan sticks, Ancβ-lineage substitutions on IF2; orange sticks, Ancβ substitutions on IF1; yellow surface, αIF2; orange surface, αIF1; green, five β substitutions close to the interfaces included in Ancα/β14 + α. **g**, nMS of Ancα/β2 across concentrations. Charge series and stoichiometries indicated. **h**, Similarity between interfaces in Ancα/β14 + Ancα homology model and X-ray crystal structure of Human Hb. Venn diagrams show sites buried at IF1 and IF2 in one or both structures. Small circle, number of shared interface sites with identical amino acid state. **i**, Hydrogen-bond contacts at interfaces in Ancα/β14 + α homology model are also found in X-ray crystal structures of extant haemoglobins. Residue pairs hydrogen-bonded in Ancα/β14 + α IF2 (yellow) and IF1 (orange) are listed; +also present in crystal structure; *interactions discussed in the main text. PDB identifiers are shown. **j**, Oxygen equilibrium curves of Ancα/β14 + α, Ancα/β4, Ancα/β2. All experiments were performed once per concentration. Lines, best-fit curves by nonlinear regression.

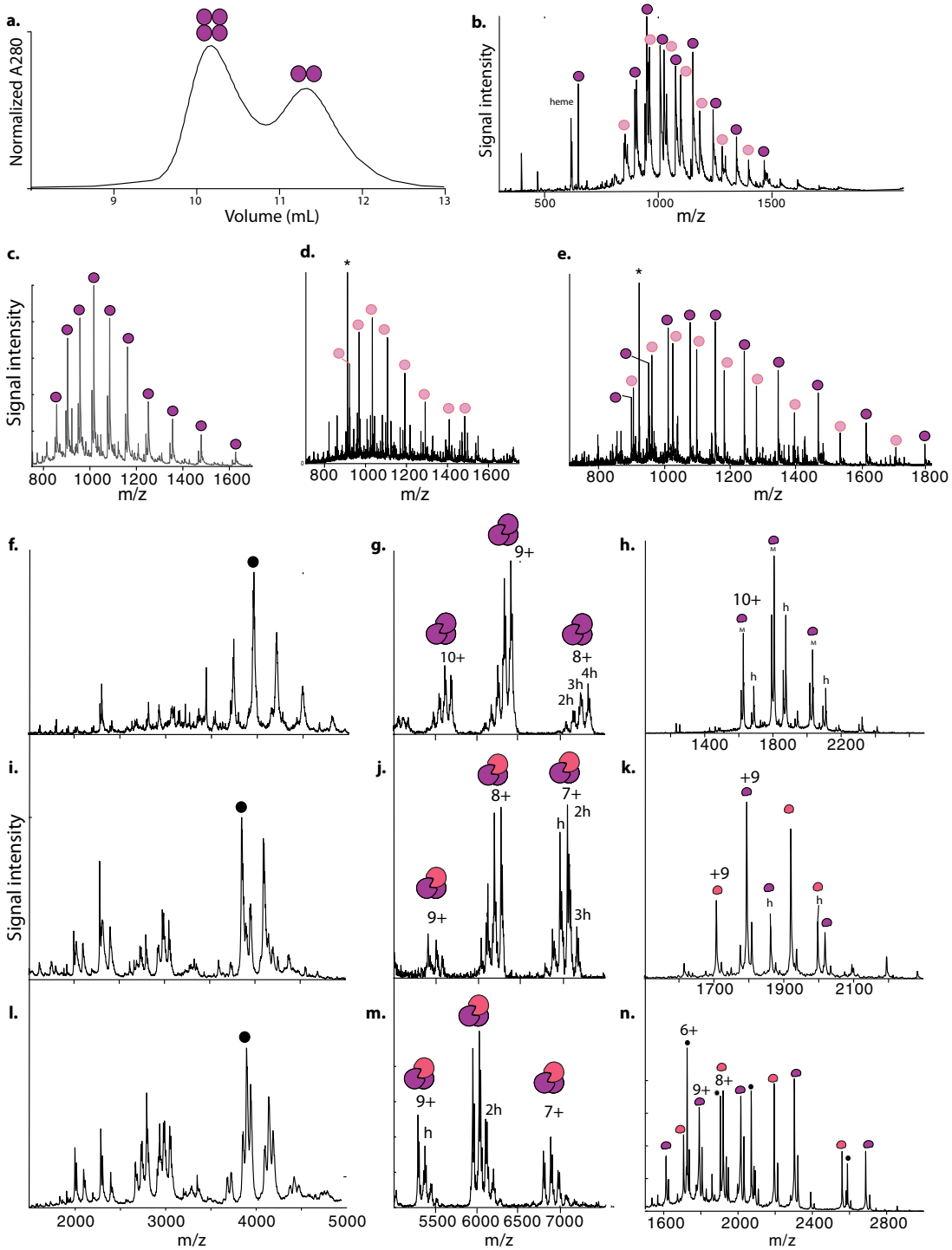

Extended Data Fig. 11 | Stoichiometric characterization of Ancα/β containing historical substitutions. a, SEC of Ancα/β5. Circles show stoichiometry associated with each peak's elution volume. **b**, High-resolution accuracy mass spectrometry (HRA-MS) of Ancα/β5 + α. Purple circles, peaks associated with Ancα/β5; pink, Ancα. **c**, HRA-MS of tetramer-containing SEC fraction of Ancα/β4 + Ancα. **d**, HRA-MS of monomer-containing SEC fraction of Ancα/β4 + Ancα. *922 *m/z* calibration reference standard. **e**, HRA-MS of Ancα/β9 + Ancα. **f**, nMS of tetramer-containing SEC fraction of Ancα/β4 + Ancα (Fig. 3a, b). Black circle, most abundant peak used for tandem MS. **g**, Tandem MS of isolated most-abundant peak in **f**, showing trimer-containing peaks. Charge states and number of haems (h) in the 8+ peak are indicated. **h**, Monomer-containing (M) peaks. **i**–**k**, nMS (**i**) and tandem MS (**j**, **k**) of Ancα/β14 + Ancα (Fig. 3f) as in **f**–**h**. **l**–**n**, nMS and tandem MS of Ancα/β5 + Ancα (Fig. 3c, d) as in **f**–**h**. Black dots in **n** mark charge species produced by cleavage of Ancα/β5. All experiments were performed once.

nature research

Corresponding author(s): Thornton

Last updated by author(s): 18/02/2020

Reporting Summary

Nature Research wishes to improve the reproducibility of the work that we publish. This form provides structure for consistency and transparency in reporting. For further information on Nature Research policies, see Authors & Referees and the Editorial Policy Checklist.

Statistics

For all statistical analyses, confirm that the following items are present in the figure legend, table legend, main text, or Methods section.

n/a	Confirmed	
☐	☒	The exact sample size (*n*) for each experimental group/condition, given as a discrete number and unit of measurement
☐	☒	A statement on whether measurements were taken from distinct samples or whether the same sample was measured repeatedly
☐	☒	The statistical test(s) used AND whether they are one- or two-sided *Only common tests should be described solely by name; describe more complex techniques in the Methods section.*
☐	☒	A description of all covariates tested
☐	☒	A description of any assumptions or corrections, such as tests of normality and adjustment for multiple comparisons
☐	☒	A full description of the statistical parameters including central tendency (e.g. means) or other basic estimates (e.g. regression coefficient) AND variation (e.g. standard deviation) or associated estimates of uncertainty (e.g. confidence intervals)
☐	☒	For null hypothesis testing, the test statistic (e.g. *F*, *t*, *r*) with confidence intervals, effect sizes, degrees of freedom and *P* value noted *Give P values as exact values whenever suitable.*
☒	☐	For Bayesian analysis, information on the choice of priors and Markov chain Monte Carlo settings
☒	☐	For hierarchical and complex designs, identification of the appropriate level for tests and full reporting of outcomes
☐	☒	Estimates of effect sizes (e.g. Cohen's *d*, Pearson's *r*), indicating how they were calculated

Our web collection on statistics for biologists contains articles on many of the points above.

Software and code

Policy information about availability of computer code

Data collection	NCBI BLAST was used to collect sequences from NCBI databases.
Data analysis	As described in the methods section, MAFFT v7 was used to build sequence alignments. PhyML 3.1 was used to infer phylogeny from globin alignment. PAML 4.1 was used to infer ancestral sequences using maximum likelihood. PyMOL v1.3 was used to visualize and render protein structures. MassHunter was used to perform mass deconvolution on high resolution accuracy mass spec. data. UNIDEC v 1.0 was used to fit molar masses to and estimate molar abundances from native mass spectrometry. SWISS-MODEL (online server: https://swissmodel.expasy.org/) and EMBO PISA v1.48 were used to model protein structures and identify protein-protein contacts. Custom scripts were used to perform statistical analyses on Hydrogen deuterium exchange data, fit dissociation constants to Native MS data and melting curves to circular dichroism data (see methods). DynamX 3.0 (Waters) was used to process HDX-MS data. OriginPro 2016 was used to fit p50s and Hill coefficient parameters to observed oxygen binding data.

For manuscripts utilizing custom algorithms or software that are central to the research but not yet described in published literature, software must be made available to editors/reviewers. We strongly encourage code deposition in a community repository (e.g. GitHub). See the Nature Research guidelines for submitting code & software for further information.

Data

Policy information about availability of data

All manuscripts must include a data availability statement. This statement should provide the following information, where applicable:

- Accession codes, unique identifiers, or web links for publicly available datasets
- A list of figures that have associated raw data
- A description of any restrictions on data availability

Reconstructed ancestral sequences have been deposited in Genbank (IDs TBA). Homology model coordinates have been deposited in the Protein Model Database (IDs TBA). Alignment and inferred phylogeny and raw mass spectra have been deposited in Dryad (URL TBA). Scripts for analysis for the HDX permutation analysis and identification of contacts between subunits in modeled structures have been deposited at github (https://github.com/JoeThorntonLab/Hb_evolution).

Field-specific reporting

Please select the one below that is the best fit for your research. If you are not sure, read the appropriate sections before making your selection.

☒ Life sciences ☐ Behavioural & social sciences ☐ Ecological, evolutionary & environmental sciences

For a reference copy of the document with all sections, see nature.com/documents/nr-reporting-summary-flat.pdf

Life sciences study design

All studies must disclose on these points even when the disclosure is negative.

Sample size	Not applicable: experiments were performed on purified stocks of recombinantly expressed proteins. Technical replication of assays is described in the manuscript.
Data exclusions	No data were excluded from the analyses.
Replication	HDX experiments were performed in 3 technical replicates per construct. Measurements of oxygen affinity, cooperativity, and allosteric regulation were performed in 3-5 technical replicates per construct. Native mass spectra and size exclusion chromatography were performed across multiple concentrations with one measurement per construct/concentration, as described in the manuscript. Error associated with replication is reported in the figures and figure legends.
Randomization	Not applicable. The experiments were performed on recombinantly expressed and purified proteins, not on individuals sampled from a population and then assigned to groups.
Blinding	Not applicable. The experiments were performed on recombinantly expressed and purified proteins, not on individuals sampled from a population and then assigned to groups.

Reporting for specific materials, systems and methods

We require information from authors about some types of materials, experimental systems and methods used in many studies. Here, indicate whether each material, system or method listed is relevant to your study. If you are not sure if a list item applies to your research, read the appropriate section before selecting a response.

Materials & experimental systems

n/a	Involved in the study
☒	☐ Antibodies
☒	☐ Eukaryotic cell lines
☒	☐ Palaeontology
☒	☐ Animals and other organisms
☒	☐ Human research participants
☒	☐ Clinical data

Methods

n/a	Involved in the study
☒	☐ ChIP-seq
☒	☐ Flow cytometry
☒	☐ MRI-based neuroimaging